Application of reverse electrodialysis to site-specific types of saline solutions: A techno-economic assessment

Article *in* Energy · May 2019

DOI: 10.1016/j.energy.2019.05.161

Francesco Giacalone
Università degli Studi di Palermo
23 PUBLICATIONS **437** CITATIONS

Michael Papapetrou
WIP Renewable Energies
39 PUBLICATIONS **1,029** CITATIONS

George Kosmadakis
RICREATION PC & NCSR "Demokritos"
91 PUBLICATIONS **2,863** CITATIONS

Alessandro Tamburini
Università degli Studi di Palermo
118 PUBLICATIONS **4,298** CITATIONS

Application of Reverse Electrodialysis to site-specific types of saline solutions: a techno-economic assessment

F. Giacalone[a], M. Papapetrou[a,b], G. Kosmadakis[b], A. Tamburini[a,*], G. Micale[a], A.Cipollina[a]

[a] Dipartimento di Ingegneria, Università degli Studi di Palermo (UNIPA) - viale delle Scienze Ed.6, 90128 Palermo-Italy.
[b] Wirtschaft und Infrastruktur GmbH & Co Planungs-KG (WIP), T *Sylvensteinstr. 2, 81369, Munich, Germany.*
Corresponding author: e–mail: alessandro.tamburini@unipa.it

ABSTRACT

Salinity gradients are a non-conventional source of renewable energy based on the recovery of the Gibbs free energy related to the mixing of solutions at different concentrations. Reverse Electrodialysis is a promising and innovative technology able to convert this energy directly into electric current. The worldwide availability of salinity gradients is limited to those locations where water bodies at different salinity levels are present. The present work analyses a number of different scenarios worldwide, in locations where salinity gradients are naturally available or generated by anthropogenic activities. A techno-economic model of the Reverse Electrodialysis process is presented. The model is used to evaluate the energy that can be harvested in each real scenario using a reverse electrodialysis plant and relevant results are reported in terms of power densities and energy yields. Finally, an economic analysis based on the estimation of the Levelized Cost Of Electricity (LCOE) for each scenario is presented, and perspective considerations are reported. Results suggest that competitive values of LCOE may be achieved in some scenarios.

KEYWORDS: *Reverse Electrodialysis, Salinity Gradient Energy, Renewable energy, Levelized Cost Of Electricity, Osmotic power, Techno-economics.*

1 INTRODUCTION

Salinity Gradient Energy (SGE) is a non-conventional renewable energy source which is attracting an increasing attention nowadays over the past few years.
Reverse Electrodialysis (RED) and Pressure Retarded Osmosis (PRO) are the main technologies able to exploit this form of energy [1]. PRO makes use of osmotic membranes to convert salinity gradients into mechanical energy which may be further converted into electricity via a hydro-turbine [2]. Conversely, RED adopts Ionic Exchange Membranes (IEMs) to directly convert the salinity gradients potential into electricity.
A significant amount of work has been recently devoted to the enhancement of the RED system performances. Efforts have been carried out to improve the performance of the IEMs reducing their electrical resistances and increasing their permselectivity [3]. The impact of different operating conditions, such as temperature [4], solution concentrations and flowrate [5], and stack configurations [6] have been experimentally studied. Several works have been focused

on the stack design, investigating the effect of (i) spacers [7] or profiled membranes [8], (ii) electrodes [9] and (iii) flow arrangements [10] on the process performance.

All these efforts led to the achievement of power densities (power per square meter of cell pair area, P_d) in the range of 12-14 W/m^2 [11]. Such values remark a significant enhancement compared to the values reported by Pattle more than 50 years ago (~0.05 W/m^2 of cell pair) [12].

Recent important achievements concern the scale-up of RED units and the operation with real solutions (as opposed to artificial NaCl solution purposely prepared in laboratories). A pilot plant consisting of three RED units with a total nominal power of 1 kW was installed in Sicily (Italy) and efficiently operated with brackish water from a well and saturated brine from a saltworks basin [13]. Very recently, Nam et al. [14], studied the largest RED unit built so far: it consists of 1000 cell pairs with 250m^2 of ionic exchange membrane area, leading to a power density of 0.76 W/m^2 of cell pair when operated with real solutions from seawater and municipal water.

The most abundant and commonly considered feed-water couple for RED systems is the combination of river-water with seawater. However, there are a number of alternative scenarios, such as the case of brine with brackish water that was above mentioned [13], where RED technology can be successfully applied achieving even higher performances. An example is the use of waste-solutions such as coal-mine [15], fish canning factory [16], pickling facility, and wastewater treatment plant [17], although suitable anti-fouling strategies must be implemented.

Other applications of Reverse electrodialysis process concern the coupling of RED stacks with conventional desalination processes for energy saving [18] or for energy storage [19], and the coupling with thermally driven regeneration units, in the so-called reverse electrodialysis heat engine [20], for converting low-grade waste heat into electricity. In the latter applications, closed loops are used and artificial solutions purposely chosen can be employed [21].

Only few works on the economical assessment of the RED technology potential applications in real environments are reported in literature. In 2007, Turek at al. [22] reported the first simplified cost estimation for the energy generated by a RED unit. By using an experimental power density value of 0.92 W/m^2 of cell pair and considering a total investment cost of 100\$/m^2 of installed membrane, they found a very high specific cost equal to 6.79\$/kWh. In 2010 Post et al. [23] presented in their analysis a prospective cost of 0.08 €/kWh assuming an installed membrane price of 2 €/m^2 (including casing and electrodes) and power density of 2 W/m^2. In 2014, Daniilidis et al. [24] carried out an economic analysis for three different RED applications (i.e. seawater, brine at 25°C and 60°C), in terms of upscaling potential using experimental P_d values. For the case of current RED units, they stated that the relevant Levelized Cost Of Electricity (LCOE) is higher than that of other competitive technologies in all the three scenarios studied. According to the same authors, (i) a future improvement of the membranes resulting into higher power density (2.7 W/m^2) and (ii) a future reduction of their specific cost (4 €/m^2) might reduce the LCOE to 0.16 €/kWh for the case of seawater-river water.

The aim of the present work is to present a fully coupled techno-economic model able to evaluate the technical potential and the economic feasibility of the RED process in different worldwide scenarios involving real water streams for feeding the RED system. More precisely, a process model extensively validated [25] is used to estimate the actual amount of energy that can be harvested from each scenario, with the relevant gross and net power densities and energy yields.

The results from the process model are used to carry out an economic analysis able to provide case by case the LCOE for three different stack sizes (0.1x0.1, 0.5x0.5 and 1.0x1.0 m^2). Furthermore, an assessment of the impact of improved membranes with higher performance and lower specific costs is made.

2 INVESTIGATED SCENARIOS

A number of scenarios were selected from locations with availability of saline water streams, as shown in Table 1. The scenarios are grouped in four categories according to their salinities: (i) seawater (SW), (ii) freshwater (FW, i.e. treated wastewater, brackish water and river water), (iii) seawater brine (SWB), and (iv) bitterns or very concentrated brines (B, i.e. saltworks brine, salty lakes), and ordered on the basis of an increasing available salinity gradient energy (see Gibbs free energy of mixing in section 3).

***Table 1**. Investigated scenarios. SW: seawater, FW: freshwater, SWB: seawater brine, B: bitterns or very concentrated brine.*

Cases	*Solutions involved (region)*	C_H [g/l]	C_L [g/l]	A_H [m^3/s]	A_L [m^3/s]
SW-FW1	**Atlantic Ocean** [26] **- Amazon river (Brazil)**[27]	35	0.04	unlimited	155 000
SW-FW2	**Adriatic Sea** [28] **-Po river (Italy)**[29]	38	0.25	unlimited	1600
SWB-FW	**Sorek SWRO plant** (5) **- TWW Tel Aviv (Israel)**(6)	70	1	2.8	4.28
B-SWB	**Dead Sea**[30,31] **– Sorek SWRO plant (Israel)** (5)	310	70	3.96	2.8
B-SW1	**Trapani saltworks brine** (1) **– Mediterranean Sea (Italy)**	280	38	0.023	unlimited
B-SW2	**Dead Sea** (2) **– Red Sea** [32] **(Jordan)**	310	41	3.96	unlimited
B-FW1	**Great Salt Lake** (3)**- TWW (Utah-US)** (4)	260	1	0.656	3.3
B-FW2	**Great Salt Lake** (3) **- Jordan River (Utah US)**	260	0.5	0.656	14.4
B-FW3	**Kara-Bogaz-Gol Bay** (7)**-Caspian Sea (Türkmenistan)**(8)	300	13.5	4.51	2708
B-FW4	**Trapani saltworks brine** (1)**- Brackish water (Italy)**	280	5.8	0.023	>0.023

(1)Total capacity 120 10^3 m^3 for 5 months/y.(2)Total capacity 114 km^3 [30,31].*(3)Total capacity 18.9 km^3* [30,33].*(4)Total capacity 75 MGD (https://www.cvwrf.org/brief-history).(5)Total capacity 411 10^3 m^3/day* [34]*, inlet flowrate evaluated assuming a recovery of 40%.(6)Total capacity 10^3 m^3/day (www.igudan.org.il/home-en/about-us/.) (7)Total capacity 130 km^3* [35].*(8)Total capacity 78200 km^3* [30,36].

The resource availability (A) (also reported in Table 1) is an important element affecting the potential of the RED process. It represents the maximum available flow rate for each considered stream. The lowest flow-rate between the two is the limiting one (Q_{lim}) for a RED plant.

The availability affects the plant size and the amount of power obtainable from the different resources. In the case of salty lakes, the maximum allowable flow rate is assumed equal to an annual volume of 0.1% of the total amount of water in the lake, in order to limit the impact of the RED system on the ecosystem. In the case of a river, the availability is set equal to 10% of the total river flowrate. In the case of saltworks brines the availability refers to 5 months per year, according to the saltworks cycle. No limitation is considered in the other cases.

2.1 Analysis of real feed waters features and related model assumptions

The scenarios investigated in the present analysis are clearly characterized by different potential mainly due to the different salinity gradient available and to the streams availability. Scenarios with higher salinity gradient, as well-known, result in higher specific energy, while the ones with larger solution availability lead to higher power output.
Each stream of the different scenarios is characterized by a number of very different features (Table 2), which could specifically affect the performance of the system. Among these, (i) ionic composition, (ii) temperature and (iii) fouling factor are those which may mostly affect the RED unit performance.

(i) Ionic composition
Each scenario is characterized by a different ionic composition of the dilute and concentrate streams: average composition of main ions is reported in Table 2. As it can be seen, in all cases the solutions contain multivalent ions. Effect of such ions on power production in RED is still an open issue in literature. Some studies report a performance reduction when bivalent ions are present in the streams (e.g. Mg^{2+}) [16]. The role of different ions on the performance of RED unit fed by real brackish water and exhausted brine from a solar pond was investigated by Tufa et al. [37]. Results indicated that large amount of Mg^{2+} ions significantly affect the performance of the system by increasing the stack resistance (+75%) and decreasing the maximum power density (-64%). Conversely, the influence of other investigated ions (i.e. HCO_3^-, K^+, $Ca^{2+}$and SO_4^{2-}) was found to produce moderate reductions (~-6%). Notably, the effect of these ions was quantified separately and for the case of the solar pond brine as a whole: the overall impact (i.e. power density reduction) did not derive from the sum of the reductions estimated per each ion, thus suggesting that ion-ion-membrane interactions may play an important role which is really difficult to quantify.
The impact of natural seawater and river water on the performance of RED system was experimentally investigated by Avci et al. [38]. Their results showed a critical effect of the real solutions on the performance of the system due to the increase of membrane resistance, the reduced OCV and the uphill transport of bivalent ions.
Overall, consolidated results on this aspect in RED units are still missing in the literature: knowledge on how ions interact among themselves and, more important, with the membranes is still poor. Without a full understanding of the reasons lying beyond the unit performance variation, it is difficult to quantify the effect of the variety of different ions contained in the natural streams. In particular, setting a specific performance variation of the RED unit for each ion concentration in each scenario was considered as a too arbitrary choice. Moreover, as reported in the literature, special-tailored membranes and/or suitable pre-treatments may reduce the impact of ions different than NaCl [3]. Thus, on the basis of the above considerations, in the present work, all streams are assumed to contain only NaCl.

The composition of the seawater (SW) is mainly given by Na^+ and Cl^- ions (~90%) with an amount of K^+, SO_4^{2-}, Mg^{2+} and Ca^{2+} ions (~10%) so small that low performance reductions due to ion composition are expected. Similar to seawater, SWRO brine (SWB) composition is dominated by Na^+ and Cl^- ions.

The composition of bitterns in each scenario can be very different. The Great Salt Lake mainly contains Na^+ and Cl^- (~87%) with few amounts of SO_4^{2-} (~7.5%) K^+ and Mg^{2+} (~5.5%). Conversely, brines (B) from Dead Sea, Marsala Saltworks and Kara-Bogaz-Gol Bay, are composed by Mg^{2+} and Na^+ (~10-18% each) cations with small amounts of Ca^{2+} and K^+, while Cl^- is the mostly abundant anion. In the scenarios concerning these bitterns, the high amount of Mg^{2+} may reduce the performance of real RED unit [37].
The composition of the fresh waters (FW) is related to the specific source, but the amount of ions contained there is so small that a significant impact of the composition on the RED unit behaviour is unexpected.

***Table 2**. Temperature, total dissolved solids and average ion composition of the streams considered in the different scenario.*

Resource	T [°C]	TDS [g/l]	Average composition of main ions [mg/l] (relative %w/w)							Ref.
			Cl^-	Na^+	Ca^{2+}	Mg^{2+}	HCO_3^-	SO_4^{2-}	K^+	
Amazon River	20-30	0.04-0.08	3.9 (9.5%)	3.1 (7.6%)	6.5 (15.9%)	1 (2.4%)	22.5 (54.9%)	3 (7.3%)	1 (2.4%)	[39]
Po river	8-15	0.1-7	1240.4 (58%)	388.7 (18.1%)	74 (3.4%)	61 (2.8%)	163.5 (7.6%)	204.2 (9.5%)	18.4 (0.9%)	[29]
Jordan river	5-30	0.3-1	148 (19.0%)	116 (14.9%)	64 (8.2%)	41 (5.3%)	228 (29.2%)	171 (21,9%)	12 (1.5%)	[40]
Typical TWW	5-30	0.1-3	315 (23%)	350 (26%)	98.4 (7%)	66.4 (5%)	330 (25%)	290 (21%)	31.5 (2%)	[41–44]
Marsala brackish water	17-27	1-5	1190 (57.2%)	410 (19.7%)	270 (13.0%)	80 (3.8%)	n/a	110 (5.3%)	20 (1.0%)	[2]
Caspian Sea	5-25	10-15	5234 (42.2%)	3016 (24.3%)	340.4 (2.7)	708.7 (5.7%)	n/a	3009.6 (24.3%)	88.4 (0.7%)	[45]
Atlantic Ocean	20-30	33-37	19374 (55.2%)	10770 (30.7%)	412.1 (1.2%)	1290 (3.7%)	140 (0.4%)	2712 (7.7%)	399 (1.1%)	[46]
Red Sea	20-31	39-41	22219 (54.4%)	14255 (34.9%)	225 (0.6%)	742 (1.8%)	146 (0.4%)	3078 (7.5%)	210 (0.5%)	[47]
Mediterranean Sea	12-26	37-38	21200 (55.4%)	11800 (30.9%)	423 (1.1%)	1403 (3.7 %)	n/a	2950 (7.7%)	463 (1.2%)	[47]
Typical SWB	15-30	50-80	38800 (52.6%)	25200 (34.2%)	814 (1.1%)	2454 (3.3%)	n/a	6463 (8.8%)	n/a	[48]
Great Salt Lake	0-26	50-350	120549.8 (55.9%)	66631 (30.9%)	377 (0.2%)	6248.3 (2.9%)	n/a	16159.5 (7.5%)	5601.9 (2.6%)	[33]
Trapani Saltworks brine	18-31	250-350	192000 (54.6%)	64000 (18.2%)	400 (0.1%)	45000 (12.8%)	n/a	39000 (11.1%)	11000 (3.1%)	[2]

Dead Sea	20-37	300-350	224000 (67.1%)	40100 (12.0%)	17650 (5.3%)	44000 (13.2%)	n/a	n/a	7650 (2.40%)	[31]
Kara-Bogaz-Gol Bay	5-25	180-390	162303 (49.7%)	53050 (16.2%)	n/a	40861 (12.5%)	2852 (0.9%)	59842 (18.3%)	7849 (2.4%)	[35]

(ii) Temperature

Some studies on how membrane performance change with the temperature are available in the literature [4]. It is well known that the higher the temperature, the higher the power produced by the RED unit. In literature, this better performance is related to an enhancement of membrane properties, but no clear relationship has been reported so far. In other words, a consolidated analysis on this aspect is still missing because the mechanisms beyond such variations are still poorly investigated. Moreover, studies at low temperature are completely missing. Thus, assuming a constant T=25°C was considered as more conservative than adding arbitrary correlations accounting for the membrane features dependence on the solution temperature.

The temperatures of seawaters investigated change during the year in the range 20-30 °C for Red Sea and tropical Atlantic Ocean while in the range 10-30 °C for Adriatic Sea.
The temperature of all bitterns ranges between a few Celsius degrees up to about 30°C, only Dead Sea temperature can reach 37°C during the summer season. Fresh water temperatures are always in the same range because their relevant inlet-point (e.g. river mouths) is located at a comparable latitude. Thus, a seasonally RED performance variation is expected, but a feed solution temperature of 25°C represents a good compromise. In other words, assuming worse performance at $T < 25°C$ and better at $T > 25°C$, no large differences are expected in the results because the average yearly temperature is not very far from 25°C in all scenarios.

(iii) Fouling

The effect of fouling on RED unit during operation has been poorly investigated so far. Only a very few papers have been devoted to investigating this issue in the literature. Kingsbury et al. tested a RED stack fed by with five different couples of real waters and wastewaters and found a large decrease of power density due to organic fouling [17]. Vermaas et al. [49] found that when no anti-fouling treatments are employed, membranes may be covered by remnants of diatoms, clay minerals, organic fouling and scaling. Di Salvo et al. [16] carried out long-run experiments by feeding a RED unit with wastewaters. The fouling issues were so severe that negative values of power (i.e. power produced lower than pumping power) were found after about one week of continuous operation. On the other hand, specific anti-fouling strategies (e.g. periodic electrodialysis-pulses, mild acidification, feeds switching, filters) can be effective and significantly reduce the fouling impact. Moreover, the adoption of profiled membranes (as in the present work) instead of spacers was found to decrease the detrimental effect of fouling [49].

Fouling factors are really site-specific. It is difficult to properly quantify the fouling potential of solutions of the same kind (e.g. two rivers may have completely different fouling features). It is even harder to quantify the potential when feeds have different nature. In general, seawaters are usually cleaner than river waters. Conversely, bacteria, algae and other organic foulants hardly reproduce and grow in very salty solutions like brines and bitterns. Particular attention

should be payed to treated waste waters (TWW) which may contain large amount of N- and P-compounds, resulting into a significant potential of biofouling phenomena.
On the basis of the above considerations, all fresh water and seawater streams were assumed to contain similar foulants which can be removed by pre-treatments units similar to those used for RO plants. As a matter of fact, these pre-treatments are expected to successfully operate for RED units as it is well-known that IEMs are less prone to fouling than osmotic membranes. Thus, suitable pre-treatments (and relevant costs) were included in the techno-economic analysis for freshwaters and seawaters. Conversely, no costly pre-treatments were considered for the brine-feeds because biological fouling is known to be reduced at large salinity values, especially at those investigated in the present scenarios. In this regard, data available for RED units fed with concentrated brines [50] show that no pre-treatments were required, except a mild filtration (to avoid large particles or precipitated salt entering the unit). Also brines coming from desalination plants are not expected to contain bio-foulants. Full details on how pre-treatments were accounted for in the economic-analysis are reported in section 4.1.2.

All the scenario-sensitive assumptions discussed so far are summarized in Table7 along with all the other techno-economic analysis assumptions.

3 THEORETICAL BACKGROUND AND MODELLING APPROACH

The maximum amount of work obtainable from the mixing of solutions at different concentration is given by the Gibbs free energy of mixing (ΔG_{mix}), which is calculated as the difference between the Gibbs free energy of the resulting solution (G_{mix}) and the one of the two original streams (G_H+G_L):

$$\Delta G_{mix} = G_{mix} - (G_H + G_L) \tag{1}$$

The Gibbs free energy of the generic i^{th} stream (G_i) is evaluated considering both water and salt contribution according to [51]. The corresponding Gibbs free power of mixing ($\Delta \dot{G}_{mix}$) can be computed from eq. 1 considering the molar flow rate (mol/s) instead of the moles of each species. The Gibbs free power of mixing is calculated by referring to equal amounts of dilute and concentrate solutions (i.e. 1 m^3/s). The specific Gibbs free energy of mixing (SME) is evaluated dividing the $\Delta \dot{G}_{mix}$ by the flow rate Q_{lim} ,which is the flowrate (in m^3/s) of the limiting (i.e. the less abundant) solution fed to the RED unit.

$$SME = \frac{\Delta \dot{G}_{mix}}{Q_{\lim}} \tag{2}$$

The operation of the RED system is simulated using a validated mathematical model already reported in the literature [25]. The model takes into account all main phenomena involved in the process, such as ion fluxes, salt and water diffusive fluxes across membranes, ohmic losses, polarization phenomena and pressure drops. A schematic representation of the RED process is reported in figure 1.

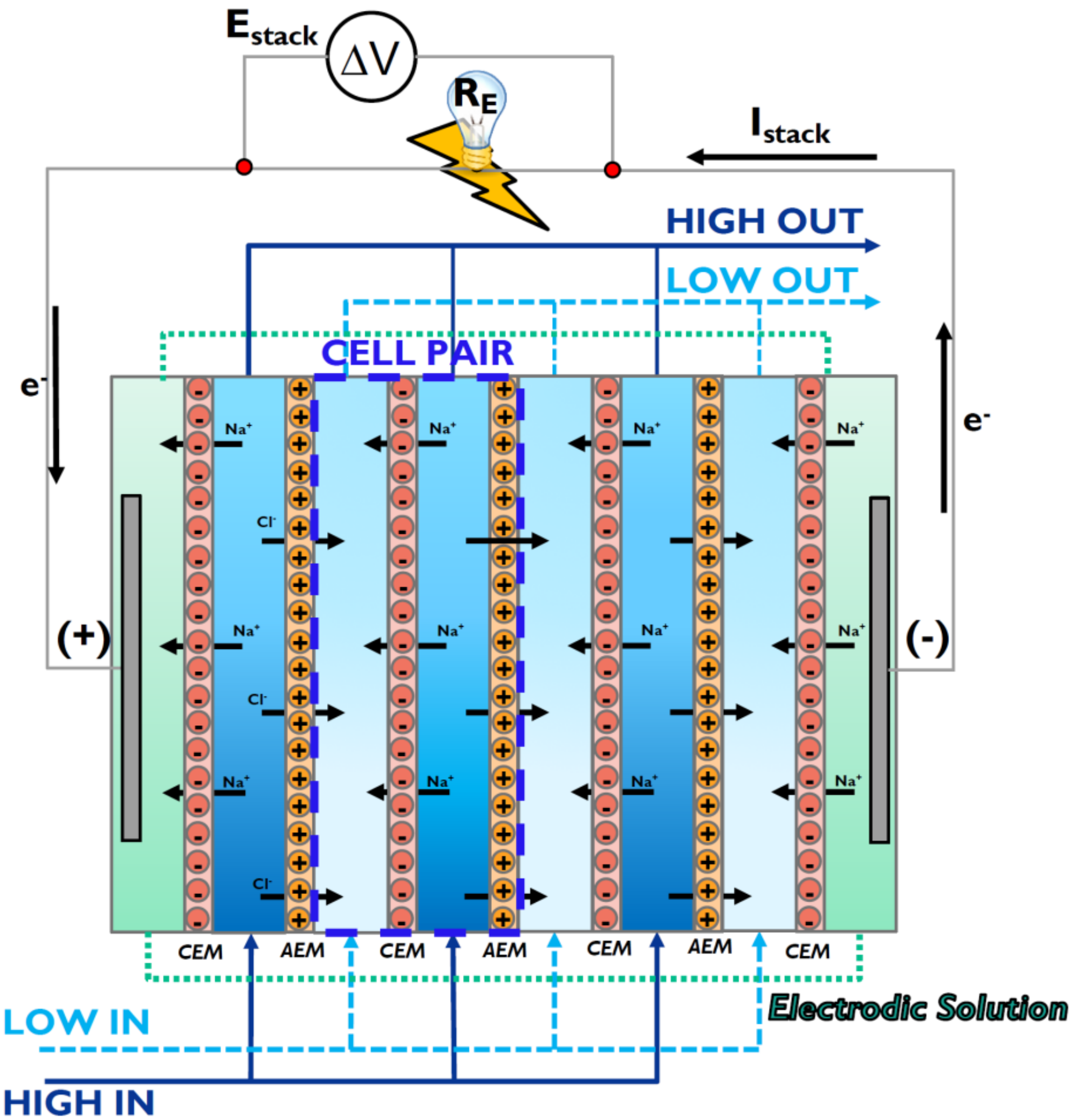

Figure 1. *Schematic representation of the RED unit*

The RED model has few simplified assumptions:

- A mono-dimensional approach was used to model RED process. Thus, the variation of all the variables (e.g. voltage, current, concentration, density, viscosity, etc.) was considered only along the main flow direction, neglecting the cross stream variation.
- All cell pairs operate in the same way, assuming an ideal flow distribution and no parasitic currents [52].
- Membrane permeability to water and salt was assumed not to be dependent on the feed stream concentrations.

Additional details on the above assumptions along with their relevant motivation are reported in Table 7.

The RED unit consists of a certain number of repetitive units named cell pairs (N_{cell}). Due to the mono-dimensional approach adopted, each cell pair is divided in N_k discretization element along the main flow direction (channel length). The voltage generated by the generic kth element of a cell pair (E_{cell}), is calculated according to eq. 3.

$$E_{cell}(k) = 2\alpha_{av}(k)\frac{RT}{zF}\ln\left(\theta_H\theta_L\frac{m_H(k)\cdot\gamma_H(k)}{m_L(k)\cdot\gamma_L(k)}\right) \tag{3}$$

in which m_{conc}, m_{dil}, γ_{conc} and γ_{dil} are the molality and activity coefficients of the two solutions, α_{av} is the average permselectivity of the two IEMs, θ_H and θ_L are the polarization coefficients which account for the concentration variation between the channel bulk and the membrane surface (see Appendix A.1), R is the universal gas constant, T is the absolute temperature (T=298 K) and F is Faraday's constant. The internal electrical resistance of the kth cell pair (R_{cell}) element consists of 4 resistances in series: the two ionic exchange membrane resistances (anionic and cationic) and the two resistances of the feed compartments (concentrate and dilute).

The electric current generated in the generic kth element of a cell pair ($i(k)$) is calculated from eq. 4:

$$i(k) = \frac{N_{cell}E_{cell}(k) - (E_{stack} + R_{blank}I_{stack})}{N_{cell}R_{cell}(k)} \tag{4}$$

where E_{stack} is the stack voltage (i.e. the externally measured electric potential of the RED unit) and R_{blank} is the resistance of the electrolyte solution compartments which can be neglected for RED stacks that have a high number of cell pairs. The electric current circulating on the external load (I_{stack}) is the sum of the ones produced in the "kth" elements (Kirchhoff's junction rule).
The closing equation is obtained by the ohm-law on the external load. The gross power ($P_{RED,gross}$) and gross power density ($P_{d,gross}$) is computed according to:

$$P_{RED,gross} = E_{stack}\cdot I_{stack} \tag{5}$$

$$P_{d,gross} = \frac{P_{RED,gross}}{N_{cell}A_{cell}} \tag{6}$$

where A_{cell} is the (active) cross section of the stack .
The net power ($P_{RED,net}$) and the net power density ($P_{d,net}$) produced by the RED unit are computed by considering the pumping power due to (i) the pre-treatments and (ii) the distributed pressure drops along the RED stack. In particular, the pumping power required for the pre-treatments (i) is evaluated according to:

$$P_{pump-pt} = \frac{N_{pt}Q_{feed}\Delta p_{pt}}{\eta_P} \tag{7}$$

where N_{pt} is the pretreatment coefficient whose values are reported in Table 6 (details on this parameter are provided in section 4.1.2), Q_{feed} is the flow-rate of the streams fed to the pre-treatment, Δp_{pt} is the pressure drop in the pre-treatment and η_p is the pump efficiency fixed to 90%. Clearly, the number of stacks to be installed in each scenario is related to the stream flowrates.

The pumping power required for the distributed pressure drop within the stack (ii) is computed on the basis of the numerical discretization adopted as the sum of the pumping power required in each k^th element, divided by the pump efficiency. In formula:

$$P_{pump-RED} = \frac{1}{\eta_P}\left(Q_H \cdot \sum_k^{N_k} \Delta p(k)_H + Q_L \cdot \sum_k^{N_k} \Delta p(k)_L\right) \tag{8}$$

where $\Delta p(k)$ is the pressure drop in each k^th discretization element evaluated according to *CFD* predictions [53]. The relevant equations are reported in Appendix A.2. Finally, the net power and power density are evaluated according to:

$$P_{RED,net} = P_{RED,gross} - P_{pump-RED} - P_{pump-pt} \tag{9}$$

$$P_{d,net} = \frac{P_{RED,net}}{N_{cp} A_{cp}} \tag{10}$$

where A_{cp} is the (active) cross section of the stack. The power and power density are functions of the external load (R_E) connected to the unit. The model includes a goal seek routine to adjust the value of external resistance maximizing the power output.

The specific energy (*SE*) for unit of limiting stream is defined as:

$$SE = \frac{P_{RED,gross}}{Q_{\lim}} \tag{11}$$

Finally, the ratio between SE and the SME is the energy yield of the process:

$$Y = \frac{SE}{SME} \tag{12}$$

The model also includes transport equations to compute the water and salt fluxes across the membranes (i.e. diffusive and migrative for the salt, osmotic and electro-osmotic for the water) and the related mass balances. These are not reported for the sake of brevity. A complete description of the model and the validation with experimental data are reported in [25].

3.1 RED specifications and parameter

Simulations were performed for each scenario by referring always to a stack with 1000 cell pairs fed by solutions flowing at 1cm/s in 155 μm channels, equipped with profiled membranes and arranged in a counter-current configuration. The influence of three different stack sizes (i.e. 0.1x0.1 m^2, 0.5x0.5 m^2 and 1.0x1.0 m^2) is investigated. Solution velocity was chosen to be equal to 1 cm/s in both the dilute and concentrate channels. Being the two channels equally thick, the flow rate of the two solutions is the same. Thus, the number of RED units which can be installed in a given scenario is obtained as the ratio of the limiting flow rate to the feed flow rate in each RED unit. A summary of the above details is reported in Figure 2.

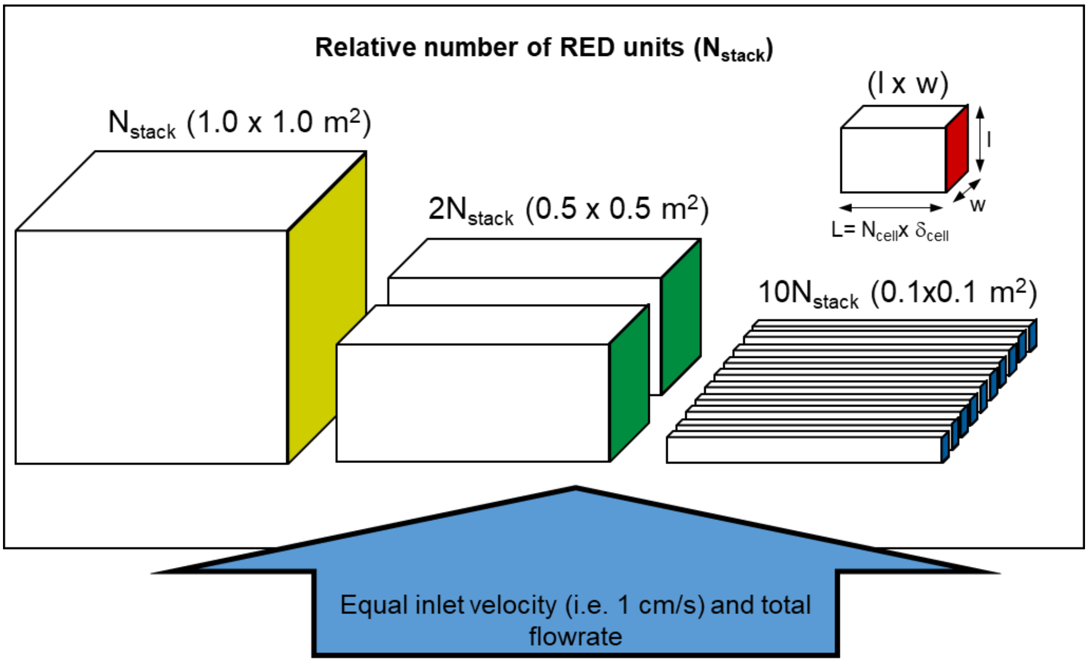

Figure 2. *Relative number of cell pairs as a function of the RED unit size. L is equal for all stacks. Coloured planes indicate the membrane plane. All stacks of the same size, as a whole manages the same overall flowrate.*

Concentration dependent correlations are used to evaluate the membrane electrical resistance and permselectivity, while constant values are used for water and salt permeability. Reference values for membranes properties are reported in Table 3, while correlations are reported in Appendix A.3. Two different sets of membranes properties are considered in the calculations, i.e. *base case* membranes (BC) and *high performing* (HP) membranes. The properties of HP membranes are assumed by improving the BC membranes. In particular, the HP membranes permselectivity is set equal to 95% (a few points higher than BC membrane permselectivity), while the other properties are set equal to ¼ of the BC ones. In the seawater-river water scenario, a further increase of permselectivity at 98% was considered because BC membranes have already permselectivity values of about 95-96%. The values of membrane electrical resistance and permselectivity adopted in this work for both BC and HP membranes are compared with literature information in fig. 3[54]. The comparison shows that values and assumptions both for the present BC and HP membranes are within the range of values reported for other IEMs.

Table 3. Base case and high performing membrane properties adopted in the analysis.

Properties	**Base case (BC)**	**High performing (HP)**
Permselectivity [%]	89[(1)]	95[(2)(3)]
Resistance [$\Omega \cdot m^2$]	3.53 10^{-04}[(1)]	8.82 10^{-05}[(1)]
Salt permeability [m^2/s]	4.5 10^{-12}[(2)]	1.1 10^{-12}[(2)]
Water Permeability [ml/(bar·h·m^2)]	8[(2)]	2[(2)]

(1)reference concentration of 2 M-0.05M NaCl water solutions. Property functions of the solution concentrations. (2)assumed constant in the whole range of concentrations. (3)equal to 98% in the case of river water-seawater.

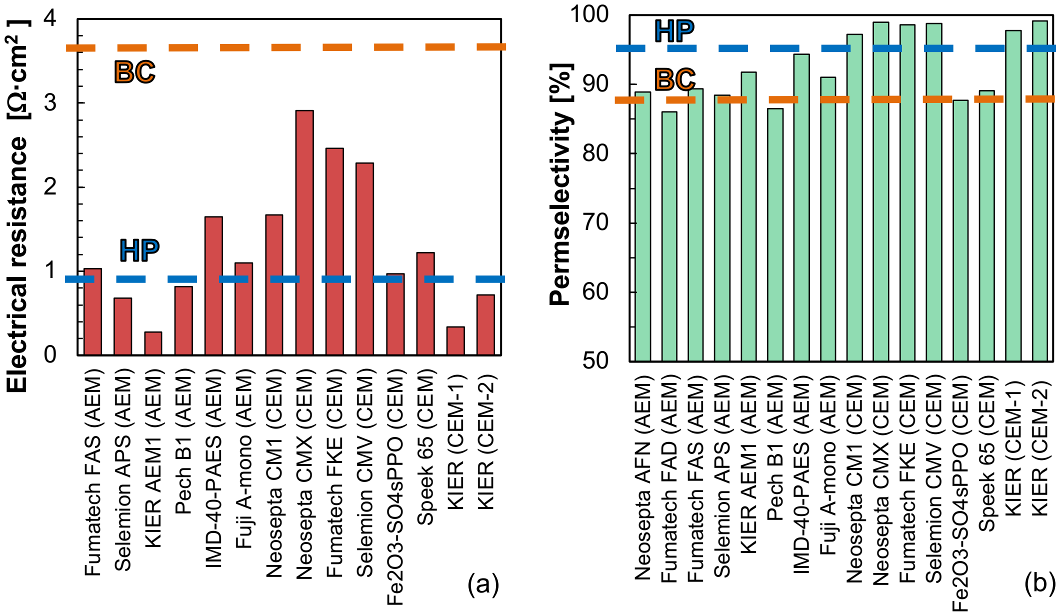

Figure 3. *Electrical resistance (a) and permselectivity (b) of available IEMs. Data from* [54].

Finally, the quantities of CO_2 emissions saved per year are evaluated by multiplying the net power generated by the RED unit times the local emission factors obtained from the literature for each scenario. The emission factors are reported in Table 4.

Table 4. *CO_2 emission factors for the different scenarios.*

Region	***kg_{CO_2}/ kWh***
Italy	0.229[(1)]
Brazil	0.093[(2)]
Middle Est	0.687[(4)]
Utah (us)	0.742[(5)]
Israel	0.740[(3)]
Turkmenistan	0.645[(3)]

(1)*https://www.eea.europa.eu/data-and-maps/indicators/overview-of-the-electricity-production-2/assessment;*
(2)*https://ecometrica.com/assets/Electricity-specific-emission-factors-for-grid-electricity.pdf;*
(3)*https://ecometrica.com/assets/Electricityspecific-emission-factors-for-grid-electricity.pdf;*
(4)*http://www.wisions.net/files/uploads/SEPS_GHG_Baseline_Calculation.pdf;*
(5)*https://www.epa.gov/sites/production/files/2018-02/documents/egrid2016_summarytables.pdf.*

4 ECONOMIC ANALYSIS

The cost of electrical energy is one of the main factors determining the readiness of a given power technology to reach the commercialization level. A large number of technologies providing electrical power is nowadays available and each of them is characterised by different working principles, operations and costs. In order to compare the cost of the electricity deriving from different power production technologies, the Levelized Cost of Electricity (LCOE) is adopted as a useful economic indicator. It represents the minimum electricity price in €/kWh required for the investment in a power generation plant to break-even over the plant lifetime. The LCOE is calculated as the ratio of the sum of the costs (including capital investment, maintenance and manufacturing costs), arising throughout the lifetime of the power plant to the sum of the produced electricity throughout the life cycle of the plant, as given by eq. 12. Due to the time-scale of the calculation, all the cost items reported in eq. 12 are discounted to their present values according to a given discount rate.

$$LCOE = \frac{\sum_{t=0}^{n} \frac{I_t + M_t}{(1+r)^t}}{\sum_{t=0}^{n} \frac{E_t}{(1+r)^t}} \tag{12}$$

where t refers to the generic year "t" with t=0 representing the start of the plant construction (a construction time of one year is assumed), n the plant lifetime, I_t the investment expenditures (capital costs) during year "t", M_t the running costs (fixed and variable operating costs) during year "t", r the discount rate, and E_t the electricity generation (in kWh) during year "t", calculated according to the capacity factor and the net power production.

Overall, the parameters considered for the cost analysis and included in eq. 12 are given in Table 5, according to estimated financial conditions for discount rate and cost factors of power plants.

Table 5. *Financial parameters*

Parameter	Value
Capacity factor	90%
Plant lifetime (t)	30 years
Discount rate (r)	5%
Other project costs	0.5% of investments
Civil and electrical infrastructure cost [55]	250 €/kW
RED membranes lifetime	10 years
RED membrane specific cost (current)	15 €/m^2_{IEM}
RED membrane specific cost (future)	4 €/m^2_{IEM}
RED electrodes	500 €/$m^2_{electrode}$
RED casing	2€/m^2_{IEM}

4.1 Capital expenditure (CAPEX)

The capital expenditure/cost (CAPEX) includes the capital cost of: (i) *RED stack*, (ii) *intake/outfall*, (iii) *pre-treatments* and (iv) *other costs* (the latter accounting for pumps, inverter, infrastructure and piping). Each cost item is presented in the following.

4.1.1 RED stack costs

The highest CAPEX contribution derives from the RED stacks, including (i) membranes, (ii) electrodes, and (iii) casing. The relevant cost for each component is reported in Table 5. As an example, for a specific membrane cost of 15 €/m^2, a stack composed of 1000 cell pairs and membrane surface of 1 m^2 costs around 35,000 € (i.e. 15·2·1000 € for membranes + 2·500 € for electrodes + 2·2·1000 € for casing). The maximum number of stacks to be installed in each scenario is calculated according to the flow rate availability of each case, as previously described.

4.1.2 Intake/outfall and pre-treatment costs

The intake/outfall and pre-treatment costs of the RED plants are estimated on the basis of similar components of reverse-osmosis (RO) seawater desalination plants.

In SWRO plants, the intake/outfall and pre-treatment costs account for 11% and 12% of the total capital costs of the plant [56], respectively. The SWRO specific cost per m^3/day of fresh water is estimated according to the expression proposed by Loutatidou et al. [57]. This specific cost is adjusted to account for the actual flow rate of the intake water (per m^3/day of intake water), using a typical water recovery ratio of 40% [58].

In order to consider the different scenarios considered, the intake/outfall capital cost is given as a fraction of the RO plant's one according to the specific conditions of each scenario examined, as each one has different requirements for intake and disposal infrastructure. In order to account for that, different coefficients have been introduced as reported in Table 6. A factor equal to 1 for each stream is used when the intake and outfall infrastructure cost is estimated to be equal to that of a RO plant. A typical example concerns the first scenario (SW-FW1), in which the specific intake/outfall cost of the RO plant is multiplied by 1.5 (1+0.5), instead of 2 (1+1). This means that for one of the two streams (seawater) entering/exiting in/from the RED plant, the cost is assumed to be the same as the RO one (factor equal to 1), while for the other stream (the river water) costs are assumed equal to half of the RO one (factor equal to 0.5).

The feed solution pre-treatment costs are calculated considering half of the pre-treatment costs needed in RO plants. In fact, electrodialysis [59,60] and reverse electrodialysis are significantly less sensitive to membrane fouling than reverse osmosis, thus requiring less pre-treatments. A scenario-sensitive approach is considered also for the calculation of the pre-treatment cost and a relevant parameter (N_{pt}) is devised. No pre-treatment costs are considered when a solution stream comes from SWRO plants, since these streams have been already treated. There are no pre-treatment costs considered in the case of brines with very high concentration since tests carried out in a RED unit fed by saltworks brines [13] indicated efficient operation without any significant pre-treatment. Therefore, in the scenario B-SWB no pre-treatment is applied for both streams (N_{pt} = 0), while in the other cases it is required for one stream only (N_{pt} = 1) or both streams (N_{pt} = 2).

Table 6. *Factors of intake/outfall and pre-treatment costs considered with respect to the reference RO intake/outfall and pre-treatment costs. SW: seawater, FW: freshwater, SWB: seawater brine, B: bittern or very concentrated brine.*

Cases	***Solutions involved (region)***	***Intake/outfall***	***Pre-treatment (N_{pt})***
SW-FW1	**Atlantic Ocean - Amazon river (Brazil)**	1.5	2
SW-FW2	**Adriatic Sea -Po river (Italy)**	1.5	2
SWB-FW	**Sorek SWRO plant - TWW Tel Aviv (Israel)**	0.4	1
B-SWB	**Dead Sea – Sorek SWRO plant (Israel)**	1.5	0
B-SW1	**Trapani saltworks brine– Mediterranean Sea (Italy)**	0.35	1
B-SW2	**Dead Sea – Red Sea (Jordan)**	2	1
B-FW1	**Trapani saltworks brine- Brackish water (Italy)**	0.35	1
B-FW2	**Great Salt Lake - TWW (Utah-US)**	0.7	1
B-FW3	**Great Salt Lake - Jordan River (Utah US)**	1	1
B-FW4	**Kara-Bogaz-Gol Bay-Caspian Sea (Türkmenistan)**	1.5	1

4.1.3 Other costs

Other costs include (i) pumps, (ii) inverter, (iii) civil & electrical infrastructure and (iv) piping costs. The pump and piping costs are calculated using the correlations provided in [61], which are derived from market prices of components with different specifications and capacities. The specific inverter cost (C_{inv}) per kW of power is given as a function of gross power production ($P_{RED,gross}$) expressed in kW according to a market research for both single-phase and three-phase inverters:

$$C_{inv} = 536.96(P_{RED,gross}[kW])^{-0.408} \tag{13}$$

The civil & electrical infrastructure cost (C_{CEI}) is fixed to 250 €/kW, as shown in Table 5.
The sum of RED stack, intake/outfall, pre-treatment and other costs constitute the total capital expenditure (CAPEX). In order to compare the operating cost with the capital one, the annualized capital cost (A_{CAPEX}) is calculated according to eq. 14.

$$A_{CAPEX} = \frac{CAPEX \cdot r \cdot (1+r)^t}{((1+r)^t - 1)} \tag{14}$$

4.2 Operating and maintenance cost (OPEX)

The main operating and maintenance costs, excluding the pumping cost and the replacement cost of the RED membranes, are assumed equal to 4% of the CAPEX as in the case of fixed OPEX of a SWRO plant [62]. The membrane replacement cost ($C_{o\text{-}IEMs}$) is evaluated on the basis of the membrane area and cost, assuming a membrane lifetime of 10 years. Pumping costs are evaluated as the product of LCOE and pumping energy requirement.

Summarizing, the techno-economic model employed described so far is based on the assumptions schematically reported in Table 7 along with their relevant motivation:

***Table** 7. Model assumptions with relevant description and motivation. Assumptions indicated by numbers should be regarded as scenario-sensitive.*

	ASSUMPTION	**DESCRIPTION**	**MOTIVATION**
1	Ideal composition of feed solutions	Each feed solution contains NaCl only	The quantification of the effect of each ion, especially of multivalent ions, on the membrane performance is still an open issue in the relevant literature.
2	Equal operating temperature in all scenarios	Each feed solution is at T=25°C	It is known that T>25°C is beneficial for the RED power generation, but quantitative characterisation is missing in the literature. Information for lower operating T is not available in literature.
3	No parasitic currents	No current is dissipated through the manifolds of the stack.	Geometrical features can be designed in order to reduce this dissipation (e.g. manifolds diameter reduction or use of "electrical baffles").
4	Constant membrane permeability to water and salt	Membrane permeability to water and salt are assumed constant at any feed solution concentration.	No specific data are available in the literature to quantify the effect of solution composition and concentration on such properties. The variation is not expected to be large.
5	Same pre-treatments for all feed solutions except brine-feeds	5a) All feed solutions, except brines, contain foulants with similar characteristics, which can be removed by pre-treatments units similar to those used for RO. 5b) No costly pre-treatments were considered for the brine-feeds.	5a) IEMs are less prone to fouling than osmotic membranes. Thus, the pre-treatments used for RO plants are expected to be more than sufficient to remove foulants for all feed-solutions. This should be regarded as a conservative assumption. 5b) Biological fouling is known to be reduced at large salinity. Brines coming from desalination plants are not expected to contain bio-foulants.
A	One dimensional model	Equations are discretized along the main flow direction only.	i) Cross-stream phenomena are less important than stream-wise ones in stacks with co-current and counter-current arrangements. 2-D model would be intrinsically essential for cross-flow stack. However, literature data show small differences between 1D and 2D models [63]. ii) Cross-stream polarization phenomena were taken into account by purposely developed correlations.
B	Equal flow rate and velocity	Feed solutions have the same flow rate, set in accordance with the limiting one. Velocity is also equal as the channel thickness is the same for the concentrate and dilute compartments.	Different feed flow rate and/or different velocity in the two channels would imply different fluid dynamics and operating conditions. This would leave room for a large number of different possibilities to be investigated and is considered out of scope for the present study.
C	Ideal Flow distribution	The solution flow rate is the same in all channels.	This assumption is realistic when pressure drops in the manifolds are low compared to the ones in the channels [64].

5 RESULTS

For each scenario, the fully integrated techno-economic model is used to analyse the performances of different RED units in terms of power production, energy yield and LCOE. In particular, (i) three different stack sizes (i.e. 0.1x0.1 m^2, 0.5x0.5 m^2 and 1.0x1.0 m^2), two different membrane property sets (i.e. base case, BC, and high performing, HP) and two different membrane specific costs (i.e. 15 €/m^2 and 4 €/m^2) were investigated.

5.1 RED unit performance

5.1.1 Energy recovery potential

Figure 4 shows a comparison of the specific Gibbs free energy of mixing (SME) for each scenario. As expected, the higher the salinity gradient between the two solutions, the higher the mixing free energy released from the mixing process. The highest SMEs are around 17 MJ/m^3 and are observed in the cases where very concentrated brine is mixed with fresh water (B-FW cases).

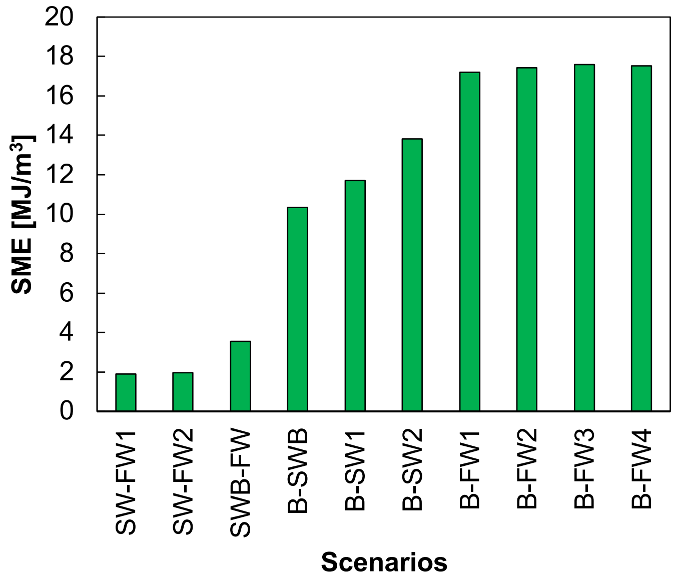

Figure 4. *Specific Gibbs free energy of mixing for the different investigated scenarios (see Table 1). The same volume of the two solutions (1 m^3) is mixed. SW: seawater, FW: freshwater, SWB: seawater brine, B: bittern or very concentrated brine.*

5.1.2 Power generation potential

Considering the theoretical power (or Gibbs free power of mixing) obtainable from each different scenario as the product of the *SME* and Q_{lim}, the source availability plays a predominant role. The highest theoretical power equal to 30 GW is obtained for the SW-FW2 case, i.e. Amazon river–Atlantic Sea. Of course, only a part of this potential can be recovered due to non-ideal and detrimental phenomena. Considering RED units consisting of 1 x 1 m^2 of membrane area, the net power generated in the SW-FW2 case, is equal to 6 GW and 10 GW adopting BC and HP membranes, respectively (fig. 5). The net power production of the system is significantly affected by the stack size, especially when small units are considered. For instance, for a size of 0.1x0.1 m^2, the–power generated in the RED unit equipped with BC membranes was found lower than the pumping power for the case of the following scenarios: SW-FW1, SW-FW2, B-SW1 and B-SW2, (relevant bars are missing in fig. 5). Clearly, different stack features and operating conditions (not investigated in the present work), suitably optimized for the worst performing scenarios could lead to positive outcomes.

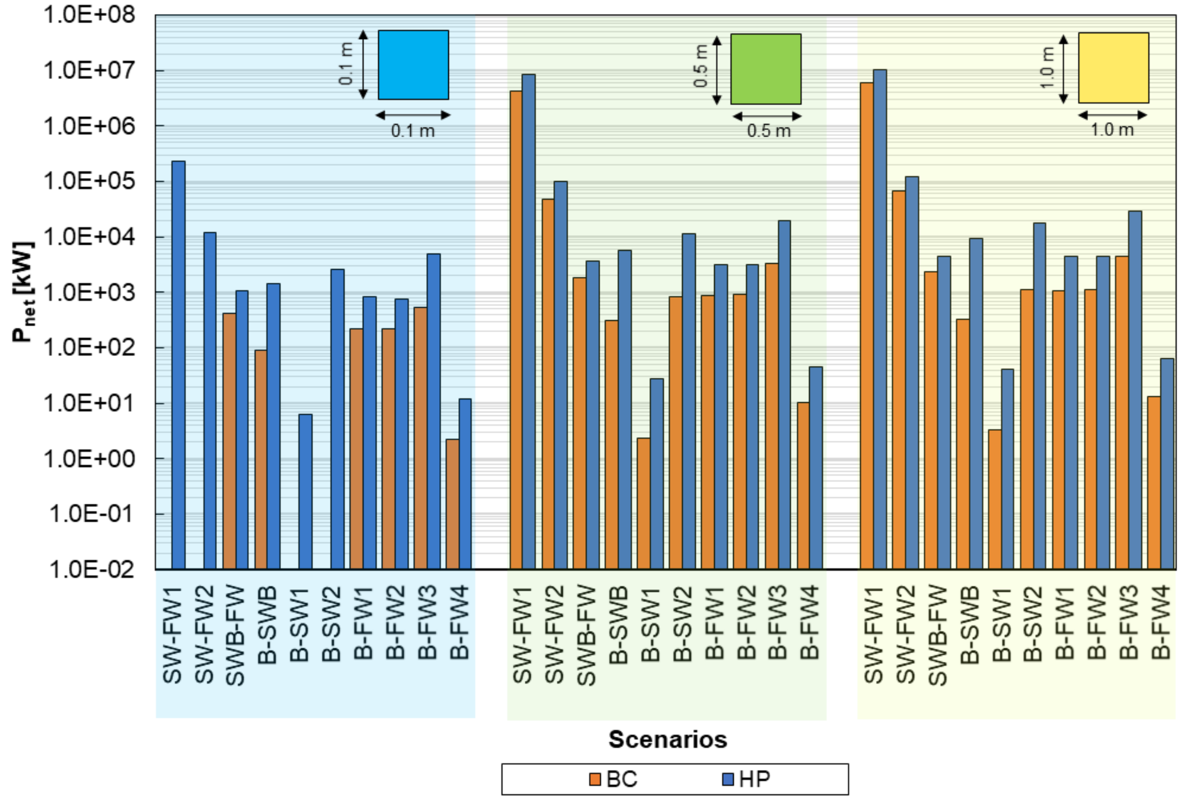

Figure 5. *Net power produced by the RED plant for the different investigated scenarios as a function of stack sizes (0.1x0.1 m^2, 0.5x0.5 m^2 and 1.0x1.0 m^2) and membranes properties (BC: base case membranes, HP: high performing membranes). Missing bars represent the scenarios where negative net powers are obtained. Solutions velocity fixed equal to 1 cm/s in all cases. Stream flowrates fixed according to source availability (see Table 1). SW: seawater, FW: freshwater, SWB: seawater brine, B: bittern or very concentrated brine.*

5.1.3 Gross power density assessment

The gross power density of the RED unit considering both BC and HP IEMs for all the investigated scenarios is reported in fig. 6 as a function of the stack size. The $P_{d,gross}$ values depend significantly on the stack length. For constant velocities (i.e. 1 cm/s in both channels), the longer the stack the lower the power density due to the driving force drop along the channels and the effect of uncontrolled mixing phenomena (i.e. water and salt diffusive fluxes). When a stack size of 0.1x0.1 m^2 is considered, the net power density in the case of river water –seawater is around 2 W/m^2_{cp} for BC membranes and 4 W/m^2_{cp} for HP membranes, while much lower values are reported for longer stacks.

The dilute solution concentration has also a significant impact on the power density. When solutions with very low conductivities are used, the dilute channel resistance represents the main resistance in the cell pair, hardly limiting the power density achievable. This detrimental effect is reduced when longer stacks are used thanks to the stream-wise concentration increase of the diluted solution. Such considerations can be inferred from fig.6 by comparing scenarios SW-FW1 and SW-FW2, where the dilute solution concentration FW2 is much more diluted than FW1.

The highest power densities, ~6 W/m^2_{cp} using BC membranes and ~19 W/m^2_{cp} adopting HP membranes, are obtained in the scenarios where very concentrated brines and fresh-water (*B-FW*) are mixed.

The $P_{d,gross}$ produced by stacks equipped with BC membranes is significantly affected by the irreversible phenomena (e.g. permselectivity, electrical resistance, water and salt flux [25]) involved in the process. The effect of resistance and permselectivity is directly related to the power generated by the unit, while water and salt fluxes affect the salinity gradient available for power production. The performance reduction is higher for the high C_H cases where driving force is higher, but (i) membranes perform worse (see for instance permselectivity correlation in Appendix A.3) and (ii) osmotic flux increases.

The scenarios where both the concentrate and the dilute solutions have the highest salinities (i.e. B-SW1, B-SW2 and B-SWB) results in a lower $P_{d,gross}$ due to the unsatisfactory membrane performance. For these scenarios, the BC IEMs permselectivity is significantly reduced up to values of 50% due to the high solution concentrations involved. Conversely, such scenarios become much more attractive when HP IEMs are employed. Increased permselectivity and reduced undesired transports (i.e. water and salt fluxes) have a significant impact. Similarly, the lower electrical resistance of HP IEMs is beneficial for these cases where C_L is so high that membrane resistance represents the main contribution to R_{stack}.

In the case of BC membranes, increasing the stack size from small to medium (i.e. 0.1x0.1 m^2 to 0.5 x0.5 m^2) leads to a power density reduction of ~30% on average. A further decrease of ~about 40% is obtained when the stack size is increased from medium to large (i.e. 0.5x0.5 m^2 to 1.0x1.0 m^2). In the case of HP membranes, a lower average reduction is observed, ~25% and ~30% respectively. This occurs because the larger the stack, the higher the residence time and the larger the impact of (i) driving force decrease and (ii) undesired transports effect.

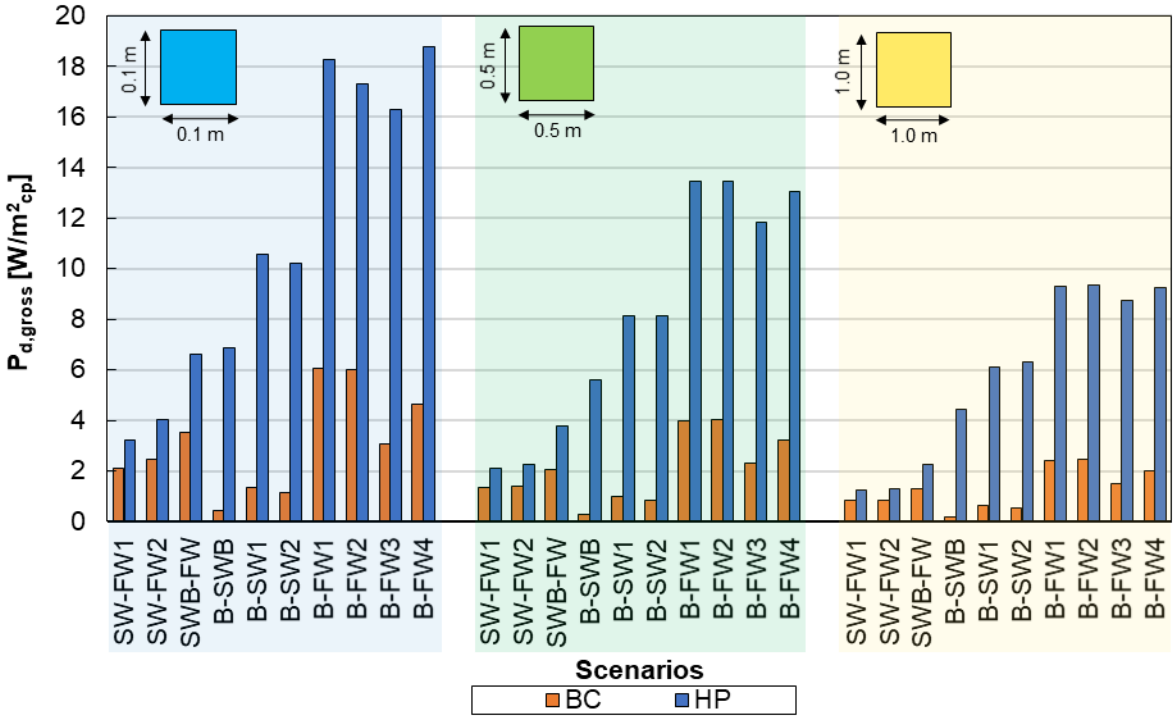

Figure 6. *$P_{d,gross}$ of the RED unit for the different investigated scenarios as a function of different stack sizes (0.1x0.1 m^2, 0.5x0.5 m^2 and 1.0x1.0m^2) and membrane properties (BC: base case membranes, HP: high performing membranes). Solutions velocity fixed equal to 1 cm/s in all cases. SW: seawater, FW: freshwater, SWB: seawater brine, B: bitterns or very concentrated brine.*

5.1.4 Energy Yield assessment

Figure 7 shows the energy yield of the RED process for each case, considering both BC and HP membranes. The energy yield (Y) represents the fraction of energy recovered in the RED unit with respect to the maximum amount available. As a difference from power density, energy yield is a growing function of solution residence time. Thus, the longer the stack, the higher the Y. For BC membranes, increasing the length of the stack from small to medium doubles the Y. A further increase from medium to large produces only a slight increase of Y (i.e ~20%), due to the progressive reduction of the available concentration difference along the channel.

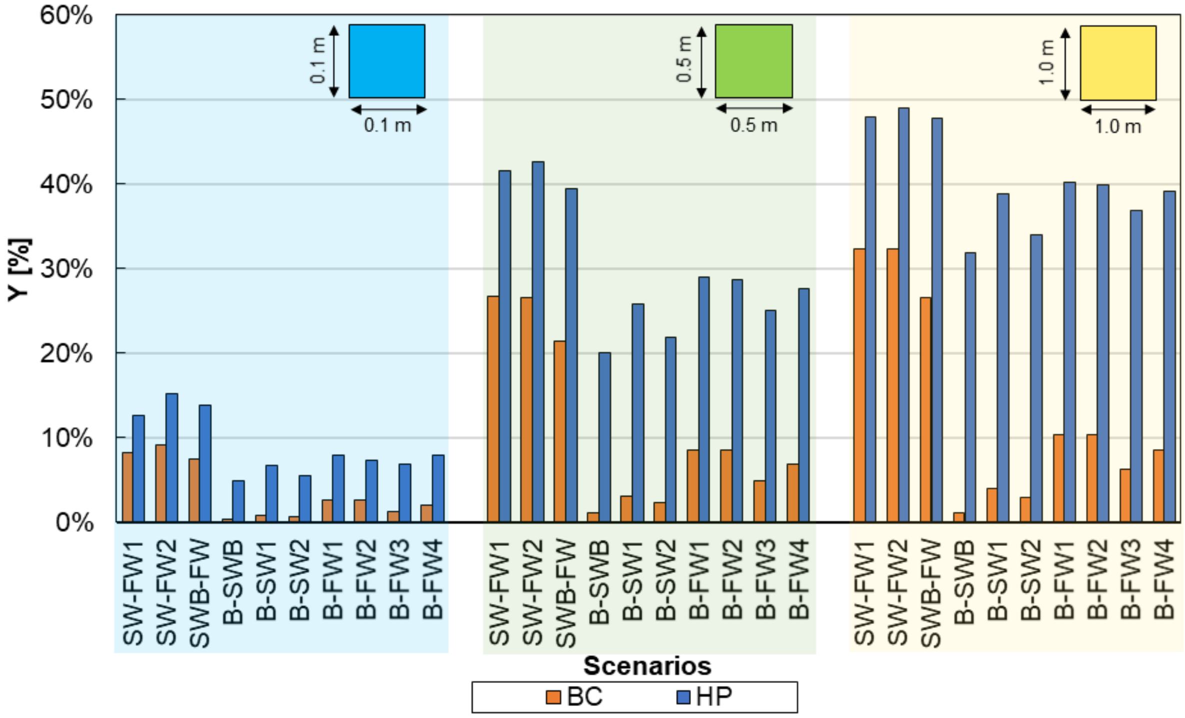

Figure 7. *Energy yield of the RED process for the different investigated scenarios as a function of different stack sizes (0.1x0.1 m², 0.5x0.5 m² and 1.0x1.0m²) and membrane properties (BC base case membranes, HP high performing membranes). Solutions velocity equal to 1 cm/s in all cases. SW: seawater, FW: freshwater, SWB: seawater brine, B: bittern or very concentrated brine.*

The energy yield is also significantly affected by the irreversibility phenomena involved in the process. For this reason, when adopting BC membranes, the highest yields (ranging between 25-30%), are obtained when the lowest salinity gradients are considered (SW-FW and SWB-FW). In these scenarios, the adoption of HP membranes produces less benefits in comparison to the cases where high C_H and/or C_L are considered.

5.2 Economic analysis

According to the methodology previously presented, LCOE values are evaluated for the three different stack sizes, considering the adoption of BC and HP membranes. A prospective analysis is also carried out considering a reduction of the membranes specific cost from 15 €/m^2 to 4 €/m^2. Results are reported in Figure 8.

5.2.1 Stack size assessment

The size of the plant is considered for each case according to the limitations imposed to the flowrate availability of the specific source, as previously described (Table 1). The LCOE is significantly affected by the stack size. The lowest LCOE values are obtained for RED unit of 0.5x0.5 m^2 due to a good compromise between power density and costs. For given stack inlet velocities (v=1cm/s) and overall flowrate to be managed, the increase of the stack size results in a proportional reduction of the number of stacks, but in an increase of available membrane area. By increasing the stack sizes from 0.1x0.1 m^2 to 0.5x0.5 m^2, the number of stacks is reduced by 5 times, but at the same time the total membrane area is 5 times larger (see fig. 2).

This increase of the membrane area results in a significant increase of the energy yield or specific energy recovered by the streams, increasing the annual production of the system by three times on scenario-average. Conversely, the power density is reduced by 30% on average. The overall result is a reduction of the LCOE of the system. However, a further increase of the stack size (i.e. from 0.5x0.5 m^2 to 1.0x1.0 m^2) results into an increase of the LCOE. This is because the small increase of net power production (see Fig. 5) and annual energy production is not enough to counterbalance the increase of the CAPEX.

5.2.2 Saline solutions assessment

In the BC membranes and stack size of 0.5x0.5 m^2, the most promising LCOEs are obtained in the cases of B-FW (fig.8). In particular, while for very low dilute concentration (i.e. C_L<6 g/l, B-FW1, BF-W2 and BFW4) the LCOE is in the range of 0.25-0.32 €/kWh, the adoption of freshwater with a higher concentration (C_L>13 g/l, B-FW3) results in higher values of LCOE (0.5 €/kWh) mainly caused by the reduction of the power density. A LCOE of 0.50 €/kWh is calculated for the case of SWB-FW, while it becomes 1.2 €/kWh for the case of SW-FW. The larger LCOE equal to 3.1 €/kWh is obtained in the case of B-SWB because of by the lower power density value.

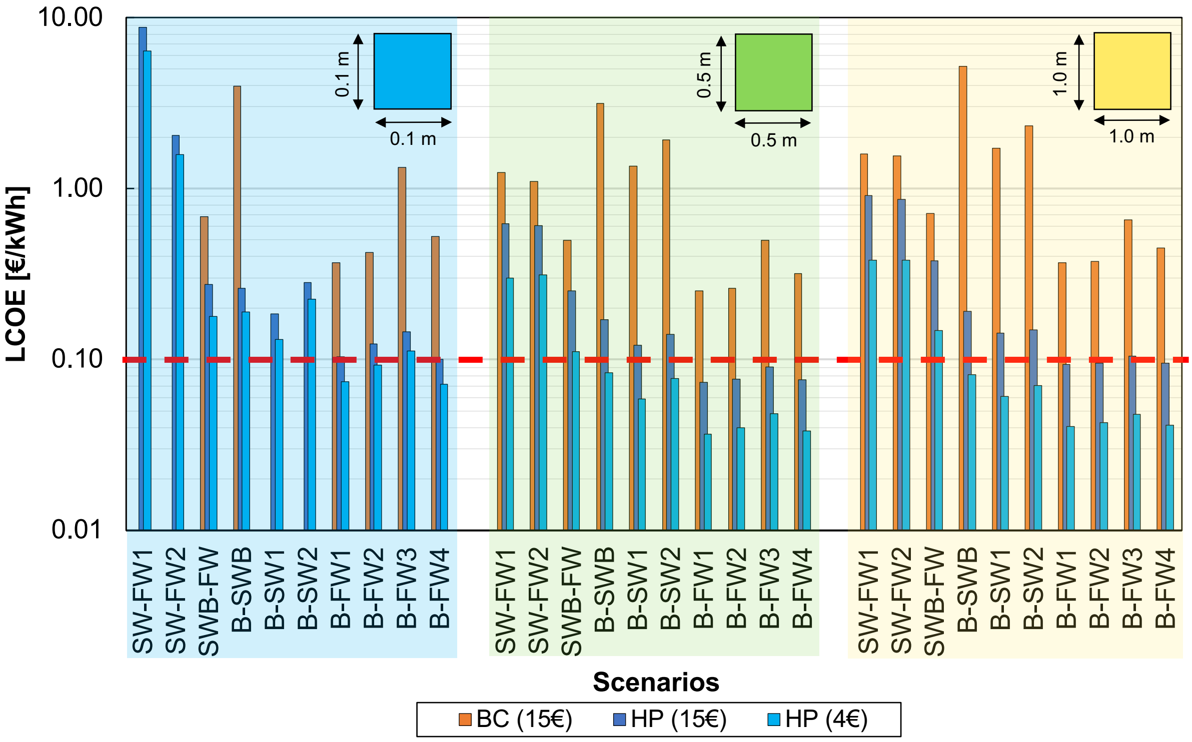

Figure 8. *LCOE of the different investigated scenarios as a function of different stack sizes (0.1x0.1 m^2, 0.5x0.5 m^2 and 1.0x1.0m^2), membrane properties (BC: base case membranes, HP: high performing membranes) and two different membrane specific prices (15€/m^2 and 4€/m^2). Solutions velocity equal to 1 cm/s in all cases. SW: seawater, FW: freshwater, SWB: seawater brine, B: bittern or very concentrated brine. Missing bars represent the scenarios where negative LCOEs are obtained.*

5.2.3 Improved membranes assessment

The adoption of HP-IEMs with a specific cost of 15 €/m^2, leads to a strong reduction of the LCOE. For the B-FW scenarios this reduction reaches values lower than the threshold value of

0.1 €/kWh (typical electricity price). This demonstrates the potential of these RED plants to become financially sustainable for a range of plant capacity: from 10 kW for the *B-FW1* case, to 3 MW for *B-FW4*.

The large benefit when using HP membranes is more clearly observed in the *B-SWB* case, for which the LCOE is reduced from 4.4 €/kWh to just 0.17 €/kWh, meaning a large impact of BC membranes properties on energy recovering from high concentration salinity gradients. In the case of HP membranes, the highest LCOE is around 0.62 €/kWh for the case of seawater-river water (SW-FW1 and SW-FW2) due to high overall costs (i.e. CAPEX and OPEX) and low specific energy.

There is still a high potential to further reduce the LCOE in case the RED membranes specific cost is reduced due to economies of scale and becomes 4 €/m^2 or even lower. In this case, the LCOE would be just 0.03-0.05 €/kWh for the most promising group represented by B-FW scenarios, considering either medium or large stack sizes. This large LCOE reduction has mostly to do with the fraction of the RED cost, contributing about 67% to the capital expenditure.

5.2.4 CAPEX and OPEX assessment

In this paragraph, a breakdown of the annual costs (i.e. CAPEX and OPEX) is presented for the case of RED units 0.5x0.5 m^2 equipped with BC membranes, as shown in Table 8.

Table 8. *Annual OPEX and CAPEX cost break-down for the BC membranes and stack size 0.5x0.5 m^2*

	CAPEX [k€/y]	OPEX [k€/y]	CAPEX				OPEX		
			$C_{c\text{-}RED}$ [%]	$C_{c\text{-}intake}$ [%]	$C_{c\text{-}pt}$ [%]	$C_{c\text{-}other}$ [%]	$C_{o\text{-}fixed}$ [%]	$C_{o\text{-}IEMs}$ [%]	$C_{pumping}$ [%]
SW-FW1	1.90E+07	6.25E+07	68.9	17.8	12.9	0.4	18.7	18.4	62.9
SW-FW2	1.84E+05	5.94E+05	73.5	15.0	10.9	0.5	19.0	20.0	61.0
SWB-FW	3.05E+03	5.46E+03	77.5	9.0	12.3	1.2	34.4	38.1	27.6
B-SWB	3.41E+03	5.60E+03	69.5	30.3	0.0	0.2	37.4	37.1	25.4
B-SW1	1.12E+01	2.84E+01	71.8	10.3	16.1	1.8	24.3	24.9	50.8
B-SW2	5.79E+03	1.51E+04	57.8	32.9	9.0	0.3	23.5	19.4	57.0
B-FW1	7.93E+02	1.16E+03	69.9	15.6	12.1	2.4	42.0	42.0	16.0
B-FW2	8.46E+02	1.20E+03	65.5	20.8	11.4	2.3	43.4	40.7	15.9
B-FW3	6.08E+03	9.61E+03	62.7	26.6	9.7	1.1	38.9	34.9	26.2
B-FW4	1.14E+01	1.75E+01	70.4	10.1	15.8	3.7	40.2	40.4	19.5
average			68.7	18.8	11.0	1.4	32.2	31.6	36.2

As far as the annual CAPEX is concerned, on average, the main expenditure is represented by the RED unit (i), with the rest divided into intake (ii), pre-treatment (iii) and other costs (iv). The RED unit cost (i) is typically in the range 60-80%, the intake cost (ii) is an important one for this type of plants, ranging from 10% to 30% of the total capital cost, while pre-treatment (iii) is in the range 10-15%. Finally, (iii) other costs contribution is always the lowest and never exceeds 4% of the total.

Concerning the OPEX, on average, the three cost components account for: (i) fixed OPEX (32%), (ii) membrane replacement cost (32 %) and pumping cost (36%).

Results highlighted that scenarios characterized by lower power density values (SW-FW, B-SW, B-SWB) are strongly affected by the pumping power costs, which are mainly due to the pumping power spent in the pre-treatment. Thus, increasing the RED unit power density or reducing the pumping power could result in a significant reduction of the LCOE.

5.2.5 CO_2 emissions assessment

Figure 9 reports the tons of CO_2 emissions saved per year in each investigated scenario. The scenarios where the streams are mostly available provide the largest CO_2 emissions saving (i.e. the scenarios with seawater and river water). This is not surprising because these scenarios provide also the highest yearly energy production.

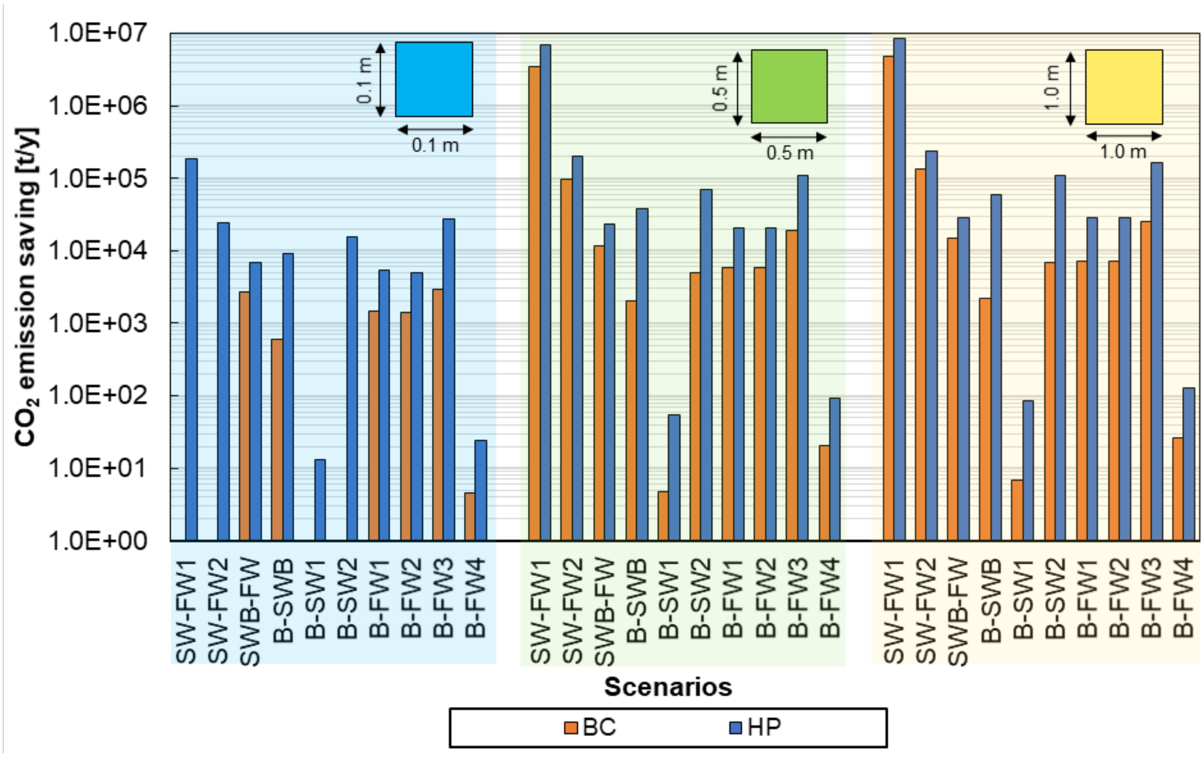

Figure 9. *Tons of CO_2 emissions saved per year in the different investigated scenarios as a function of different stack sizes (0.1x0.1 m^2, 0.5x0.5 m^2 and 1.0x1.0 m^2) and membrane properties (BC base case membranes, HP high performing membranes). Solutions velocity equal to 1 cm/s in all cases. SW: seawater, FW: freshwater, SWB: seawater brine, B: bittern or very concentrated brine. Missing bars represent the scenarios where negative CO_2 emission saving are obtained*

6 CONCLUSIONS

Reverse electrodialysis is a novel technology to harvest the energy related to the mixing of streams at different salinity levels. The present work investigates the technology potential by analysing its application to some specific real case studies around the world, considering the current state of the art of the technology and a prospective analysis implying future improved membranes.

The potential of the reverse electrodialysis unit depends on the solution driving force and availability (i.e. usable flow-rates). Three different stack sizes are considered in the analysis in order to study the effect of residence time and available membrane area. In general, the medium stack size of 0.5x0.5 m^2 is the best performing.

For all the investigated scenarios the Levelized Cost of Electricity (LCOE) is calculated. As results of the analysis, the LCOE is significantly affected by the available salinity gradient, membrane properties, specific membrane cost and energy spent on pumping. Using base case membranes and specific membrane cost of 15 €/m^2, the lowest LCOE, ranging from 0.27 to 0.33 €/kWh, is obtained when brine and freshwater are used. Higher LCOE values are obtained for the other scenarios. The adoption of high performing membranes accompanied by a future cost reduction can lead to a competitive LCOE, lower than 0.10 €/kWh, for a number of investigated scenarios. In particular the "brine-fresh water" scenarios provide the lowest LCOE. This demonstrates the potential of brine-fresh water RED plants to become financially sustainable for a range of plant capacity: from ~40 kW for the B-FW1 case (i.e. Italy: Trapani saltworks brine - Brackish water), to ~20 MW for B-FW4 scenario (i.e. Türkmenistan: Kara-Bogaz-Gol Bay - Caspian Sea). Clearly, higher values of power can be produced if a higher stream availability is considered: only a low exploitation of the resources is considered in the present work.

It is also worth noting that all the scenarios where the calculated LCOE (even with cheap High Performing membranes) is non-competitive should not be discarded for future studies because stack features and operating conditions suitably optimized for each scenario could result into different outcomes.

On overall, the results of this work suggest that there is room for further improvements on many aspects. Membranes are the key-process items and further studies from researchers and manufacturers are needed in order to improve their performance at an affordable cost. Additional data are needed to help modellers to account for phenomena such as membrane fouling, parasitic currents, transport of ions different from Na^+ and Cl^-. Once all these phenomena have been fully understood and properly accounted for, relevant models will be used to guide the design of the stack maximizing the exploitation of the available salinity gradient source. Moving towards a fine technical and economical optimization should be regarded as the only way to make reverse electrodialysis technology competitive in a number of different scenarios.

NOMENCLATURE

Symbols

A	Availability of the stream [m^3/s]
A_{CAPEX}	Annualized CAPEX (€/y)
A_{cell}	Cell pair membrane area (m^2)
$CAPEX$	Capital expenditures (€)
$C_{c\text{-}intake}$	CAPEX intake/outfall cost (€)
$C_{c\text{-}other}$	CAPEX other cost (€)
$C_{c\text{-}pt}$	CAPEX pre-treatment cost (€)
$C_{c\text{-}RED}$	CAPEX RED stacks cost (€)
$e2$	Civil & electrical infrastructure cost (250 €/kW)
C_H	Concentrate Molar Concentration (g/l)
C_{inv}	Inverters cost (€)
C_L	Dilute Molar Concentration (g/l)
$C_{o\text{-}fixed}$	OPEX fixed cost (€/y)
$C_{o\text{-}IEM}$	OPEX membrane replacement cost (€/y)
$C_{pumping}$	Equivalent global pumping cost (€/y)
D	Diffusivity (m^2/s)
D_{eq}	Equivalent diameter (m)
E_{cell}	Voltage generated by the cell pair (V)
E_{stack}	Voltage generated by the pile (V)
E_t	Electricity generation (kWh)
F	Faraday constant (C/mol)
f_{Darcy}	Friction factor
G	Gibbs free energy (kJ)
$i(k)$	Electrical current in the k^{th} element (A)
I_{stack}	Electric current circulating in the external circuit(A)
I_t	Investment expenditures in the year t (€)
J_{tot}	Global salt flux (mol/(m^2 s))
k	Discretization element
$LCOE$	Livelized Cost of electricity (€/kWh)
m	Molality (mol/kg_{solv})
M_t	Running cost in the year t (€)
n	Number of moles (mol)
N_{cell}	Number of cell pair
N_k	Number of discretization elements
N_{pt}	Pre-treatment coefficient
N_{stack}	Number of stacks
OCV	Open circuit voltage
$OPEX$	Operating expenditures (€/y)
P_d	RED Power density (W/m^2)
P_{loss}	Pumping power required (W)

$P_{pump\text{-}pt}$	Pre-treatment pumping power (W)
$P_{pump\text{-}RED}$	RED pumping power (W)
P_{RED}	RED power (W)
Q	Volumetric Flowrate (m^3/s)
Q_{lim}	Flowrate of the limiting source (m^3/s)
R	Universal Gas constant (J/(K mol))
r	Discount ratio
R_{blamk}	Electrical resistance of the electrodic compartment (Ω)
R_{cell}	Electrical resistance of the cell pair (Ω)
R_E	Load Resistance (Ω)
Re	Reynolds number
R_H	Electrical resistance of concentrate (Ωm^2)
R_{IEM}	Ionic exchange membrane resistance (Ωm^2)
R_L	Electrical resistance of dilute (Ωm^2)
Sc	Schmidt number
SE	Net Specific Energy (kJ/m^3)
Sh	Sharwood number
SME	Specific Gibbs free energy of mixing per unit of concentrate (MJ/m^3)
T	Temperature (°C or K)
t	Plant lifetime (years)
v	Solution velocity (m/s)
Y	Energy Yield
z	Ion charge

Greek symbols

θ	Polarization coefficient
Δx	Length of the discretization element (m)
α	Permselectivity
γ	Salt activity coefficient
ΔG_{mix}	Gibbs free energy of mixing (kJ)
$\Delta p(k)$	Element pressure drop in the RED channel (bar)
μ	Chemical potential of the generic i species (kJ/mol)
ρ	Density ($kg/m^{3)}$
δ	Channel thickness (m)
δ_{cell}	Cell pair thickness (m)
η_p	Pump efficiency

Subscripts

av	Related to Average property
b	Related to the solution bulk
cp	Related to the cell pair
feed	Related to the total feed flowrate in the pre-treatment

gross	Related to gross value
H	Related to the concentrate stream
L	Related to the dilute stream
lim	Related to the limiting stream
m	Related to the membrane interphase
net	Related to net consumptions
pt	Related to the pre-treatment

Acronyms

B	Bitterns
BC	Base case membranes
CFD	Computational fluid dynamics
FW	Fresh water
HP	High performing membranes
IEM	Ionic Exchange Membrane
LCOE	Levelized Cost Of Electricity
PRO	Pressure Retarded Osmosis
RED	Reverse Electrodialysis
RO	Reverse Osmosis
SGE	Salinity Gradient Energy
SW	Seawater
SWB	Seawater reverse osmosis brine
SWRO	Seawater reverse osmosis
TDS	Total dissolved solid
TWW	Treated wastewater

REFERENCES

[1] G.L. Wick, Power from salinity gradients, Energy. 3 (1978) 95–100. doi:10.1016/0360-5442(78)90059-2.

[2] A. Cipollina, G. Micale, Sustainable energy from salinity gradients, Elsevier Ltd, 2016. doi:10.1016/C2014-0-03709-4.

[3] R.A. Tufa, S. Pawlowski, J. Veerman, K. Bouzek, E. Fontananova, G. di Profio, S. Velizarov, J. Goulão Crespo, K. Nijmeijer, E. Curcio, Progress and prospects in reverse electrodialysis for salinity gradient energy conversion and storage, Appl. Energy. 225 (2018) 290–331. doi:10.1016/j.apenergy.2018.04.111.

[4] A.M. Benneker, T. Rijnaarts, R.G.H. Lammertink, J.A. Wood, Effect of temperature gradients in (reverse) electrodialysis in the Ohmic regime, J. Memb. Sci. 548 (2018) 421–428. doi:10.1016/j.memsci.2017.11.029.

[5] M. Tedesco, E. Brauns, A. Cipollina, G. Micale, P. Modica, G. Russo, J. Helsen, Reverse electrodialysis with saline waters and concentrated brines: A laboratory investigation towards technology scale-up, J. Memb. Sci. 492 (2015) 9–20. doi:10.1016/j.memsci.2015.05.020.

[6] J. Veerman, R.M. de Jong, M. Saakes, S.J. Metz, G.J. Harmsen, Reverse

electrodialysis: Comparison of six commercial membrane pairs on the thermodynamic efficiency and power density, J. Memb. Sci. 343 (2009) 7–15. doi:10.1016/j.memsci.2009.05.047.
[7] M. Ciofalo, M. La Cerva, Massimiliano Di Liberto, L. Gurreri, A. Cipollina, G. Micale, Optimization of net power density in Reverse Electrodialysis, Energy. (2019) under review.
[8] L. Gurreri, M. Ciofalo, A. Cipollina, A. Tamburini, W. Van Baak, G. Micale, CFD modelling of profiled-membrane channels for reverse electrodialysis, Desalin. Water Treat. 55 (2015) 3404–3423. doi:10.1080/19443994.2014.940651.
[9] O. Scialdone, C. Guarisco, S. Grispo, A.D. Angelo, A. Galia, Investigation of electrode material – Redox couple systems for reverse electrodialysis processes. Part I: Iron redox couples, J. Electroanal. Chem. 681 (2012) 66–75. doi:10.1016/j.jelechem.2012.05.017.
[10] D.A. Vermaas, J. Veerman, N.Y. Yip, M. Elimelech, M. Saakes, K. Nijmeijer, High efficiency in energy generation from salinity gradients with reverse electrodialysis, ACS Sustain. Chem. Eng. 1 (2013) 1295–1302. doi:10.1021/sc400150w.
[11] A. Daniilidis, D.A. Vermaas, R. Herber, K. Nijmeijer, Experimentally obtainable energy from mixing river water, seawater or brines with reverse electrodialysis, Renew. Energy. 64 (2014) 123–131. doi:10.1016/j.renene.2013.11.001.
[12] R.E. Pattle, Production of Electric Power by mixing Fresh and Salt Water in the Hydroelectric Pile, Nature. 174 (1954) 660–660. doi:10.1038/174660a0.
[13] M. Tedesco, A. Cipollina, A. Tamburini, G. Micale, Towards 1 kW power production in a reverse electrodialysis pilot plant with saline waters and concentrated brines, J. Memb. Sci. 522 (2017) 226–236. doi:10.1016/j.memsci.2016.09.015.
[14] J.-Y. Nam, K.-S. Hwang, H.-C. Kim, H. Jeong, H. Kim, E. Jwa, S. Yang, J. Choi, C.-S. Kim, J.-H. Han, N. Jeong, Assessing the behavior of the feed-water constituents of a pilot-scale 1000-cell-pair reverse electrodialysis with seawater and municipal wastewater effluent, Water Res. 148 (2019) 261–271. doi:10.1016/j.watres.2018.10.054.
[15] M. Turek, B. Bandura, P. Dydo, Power production from coal-mine brine utilizing reversed electrodialysis, 221 (2008) 462–466. doi:10.1016/j.desal.2007.01.106.
[16] J. Luque Di Salvo, A. Cosenza, A. Tamburini, G. Micale, A. Cipollina, Long-run operation of a reverse electrodialysis system fed with wastewaters, J. Environ. Manage. 217 (2018) 871–887. doi:10.1016/j.jenvman.2018.03.110.
[17] R.S. Kingsbury, F. Liu, S. Zhu, C. Boggs, M.D. Armstrong, D.F. Call, O. Coronell, Impact of natural organic matter and inorganic solutes on energy recovery from five real salinity gradients using reverse electrodialysis, J. Memb. Sci. 541 (2017) 621–632. doi:10.1016/j.memsci.2017.07.038.
[18] M. Chen, Y. Mei, Y. Yu, R.J. Zeng, F. Zhang, S. Zhou, C.Y. Tang, An internal-integrated RED/ED system for energy-saving seawater desalination: A model study, Energy. 170 (2019) 139–148. doi:10.1016/j.energy.2018.12.111.
[19] W.J. Van Egmond, M. Saakes, S. Porada, T. Meuwissen, C.J.N. Buisman, H.V.M. Hamelers, The concentration gradient flow battery as electricity storage system: Technology potential and energy dissipation, J. Power Sources. 325 (2016) 129–139. doi:10.1016/j.jpowsour.2016.05.130.
[20] F. Giacalone, C. Olkis, G. Santori, A. Cipollina, S. Brandani, G. Micale, Novel solutions for closed-loop reverse electrodialysis: Thermodynamic characterisation and perspective analysis, Energy. 166 (2019) 674–689. doi:10.1016/j.energy.2018.10.049.
[21] M. Bevacqua, A. Tamburini, M. Papapetrou, A. Cipollina, G. Micale, A. Piacentino, Reverse electrodialysis with NH4HCO3-water systems for heat-to-power conversion,

Energy. 137 (2017) 1293–1307. doi:10.1016/j.energy.2017.07.012.
[22] M. Turek, B. Bandura, Renewable energy by reverse electrodialysis, 205 (2007) 67–74. doi:10.1016/j.desal.2006.04.041.
[23] J.W. Post, C.H. Goeting, J. Valk, S. Goinga, J. Veerman, H.V.M. Hamelers, P.J.F.M. Hack, Towards implementation of reverse electrodialysis for power generation from salinity gradients, Desalin. Water Treat. 16 (2010) 182–193. doi:10.5004/dwt.2010.1093.
[24] A. Daniilidis, R. Herber, D.A. Vermaas, Upscale potential and financial feasibility of a reverse electrodialysis power plant, Appl. Energy. 119 (2014) 257–265. doi:10.1016/j.apenergy.2013.12.066.
[25] F. Giacalone, P. Catrini, A. Tamburini, A. Cipollina, A. Piacentino, G. Micale, Exergy analysis of reverse electrodialysis, Energy Convers. Manag. 164 (2018) 588–602. doi:10.1016/j.enconman.2018.03.014.
[26] J.F. Ternon, C. Oudot, A. Dessier, D. Diverres, A seasonal tropical sink for atmospheric CO2 in the Atlantic ocean: The role of the Amazon River discharge, Mar. Chem. 68 (2000) 183–201. doi:10.1016/S0304-4203(99)00077-8.
[27] E.A. Ríos-Villamizar, M.T.F. Piedade, J.G. Da Costa, J.M. Adeney, W.J. Junk, Chemistry of different Amazonian water types for river classification: A preliminary review, WIT Trans. Ecol. Environ. 178 (2013) 17–28. doi:10.2495/WS130021.
[28] S. Covelli, J. Faganeli, M. Horvat, A. Brambati, Mercury contamination of coastal sediments as the result of long-term cinnabar mining activity (Gulf of Trieste, northern Adriatic sea), Appl. Geochemistry. 16 (2001) 541–558. doi:10.1016/S0883-2927(00)00042-1.
[29] C. Marchina, G. Bianchini, C. Natali, M. Pennisi, N. Colombani, R. Tassinari, K. Knoeller, The Po river water from the Alps to the Adriatic Sea (Italy): new insights from geochemical and isotopic (δ18O-δD) data, Environ. Sci. Pollut. Res. 22 (2015) 5184–5203. doi:10.1007/s11356-014-3750-6.
[30] C.E. Herdendorf, Large Lakes of the World, J. Great Lakes Res. 8 (1982) 379–412. doi:10.1016/S0380-1330(82)71982-3.
[31] R.A.I. Bashitialshaaer, K.M. Persson, M. Larson, Mixing Time for the Dead Sea Based on Water and Salt Mass Balances, Euromed 2008 Coop. among Mediterr. Ctries. Eur. MENA Reg. (2008).
[32] R.A.I. Bashitialshaaer, K.M. Persson, M. Aljaradin, Estimated future salinity in the Arabian Gulf, the Mediterranean Sea and the Red Sea concequences of brine discharge from desalination, Intrenational J. Acad. Res. 3 (2011) 133–140.
[33] I.N. Mohammed, Modeling the Great Salt Lake, Statew. Agric. L. Use Baseline 2015. 1 (2015). doi:10.1017/CBO9781107415324.004.
[34] F. Lokiec, Sorek 150 million m^3/year seawater desalination facility build, operate and transfer (BOT) project. Paper presented at the IDA World Congress, Perth Convention and Exhibition Centre (PCEC), Perth, 4–9 September 2011, IDA World Congr. - Perth, West. Aust. Sept. 4-9, 2011. (2011) 1–15.
[35] A.N. Kosarev, A.G. Kostianoy, I.S. Zonn, Kara-Bogaz-Gol bay: Physical and chemical evolution, Aquat. Geochemistry. 15 (2009) 223–236. doi:10.1007/s10498-008-9054-z.
[36] A.G. Pervov, A.P. Andrianov, R. V. Efremov, A. V. Desyatov, A.E. Baranov, A new solution for the Caspian Sea desalination: Low-pressure membranes, Desalination. 157 (2003) 377–384. doi:10.1016/S0011-9164(03)00420-X.
[37] R.A. Tufa, E. Curcio, W. Van Baak, J. Veerman, S. Grasman, E. Fontananova, G. Di Profio, Potential of brackish water and brine for energy generation by salinity gradient power-reverse electrodialysis (SGP-RE), RSC Adv. 4 (2014) 42617–42623. doi:10.1039/c4ra05968a.

[38] A.H. Avci, R.A. Tufa, E. Fontananova, G. Di Profio, E. Curcio, Reverse Electrodialysis for energy production from natural river water and seawater, Energy. 165 (2018) 512–521. doi:10.1016/j.energy.2018.09.111.
[39] R.J. Gibbs, Water chemistry of the Amazon River, Geochim. Cosmochim. Acta. 36 (1972) 1061–1066.
[40] R. April, Geochemistry of Great Salt Lake , Utah I : Hydrochemistry since 1850, Geochim. Cosmochim. Acta. 49 (1985) 727–737.
[41] L. Gharbi, P. Merdy, M. Raynaud, H. Pfeifer, Y. Lucas, Applied Geochemistry Effects of long-term irrigation with treated wastewater . Part I : Evolution of soil physico-chemical properties, Appl. Geochemistry. 25 (2010) 1703–1710. doi:10.1016/j.apgeochem.2010.08.018.
[42] J. Tahtouh, R. Mohtar, A. Assi, P. Schwab, A. Jantrania, Y. Deng, C. Munster, Impact of brackish groundwater and treated wastewater on soil chemical and mineralogical properties, Sci. Total Environ. 647 (2019) 99–109. doi:10.1016/j.scitotenv.2018.07.200.
[43] P.C.P. de Oliveira, T.V. Gloaguen, R.A.B. Gonçalves, D.L. Santos, C.F. Couto, Soil Chemistry after Irrigation with Treated Wastewater in Semiarid Climate, Rev. Bras. Ciência Do Solo. 40 (2016) 1–13. doi:10.1590/18069657rbcs20140664.
[44] S. Bedbabis, D. Trigui, C. Ben Ahmed, M.L. Clodoveo, S. Camposeo, G.A. Vivaldi, B. Ben Rouina, Long-terms effects of irrigation with treated municipal wastewater on soil, yield and olive oil quality, Agric. Water Manag. 160 (2015) 14–21. doi:10.1016/j.agwat.2015.06.023.
[45] F. Peeters, R. Kipfer, D. Achermann, M. Hofer, U. Beyerle, D.M. Imboden, K. Rozanski, K. Fro, Analysis of deep-water exchange in the Caspian Sea based on environmental tracers, Deep. Res. 47 (2000) 621–654.
[46] M. Pontié, J.S. Derauw, S. Plantier, L. Edouard, L. Bailly, Seawater desalination: nanofiltration—a substitute for reverse osmosis?, Desalin. Water Treat. 51 (2013) 485–494. doi:10.1080/19443994.2012.714594.
[47] Lenntech, (2017). https://www.lenntech.com/composition-seawater.htm.
[48] M. Meneses, J.C. Pasqualino, R. Céspedes-Sánchez, F. Castells, F Alternatives for Reducing the Environmental Impact of the Main Residue From a Desalination Plant. J. Ind. Ecol. 14 (2010), 512–527.
[49] D.A. Vermaas, D. Kunteng, M. Saakes, K. Nijmeijer, Fouling in reverse electrodialysis under natural conditions, Water Res. 47 (2012) 1289–1298. doi:10.1016/j.watres.2012.11.053.
[50] M. Tedesco, C. Scalici, D. Vaccari, A. Cipollina, A. Tamburini, G. Micale, Performance of the first reverse electrodialysis pilot plant for power production from saline waters and concentrated brines, J. Memb. Sci. 500 (2016) 33–45. doi:10.1016/j.memsci.2015.10.057.
[51] K.S. Pitzer, J.C. Peiper, R.H. Busey, Thermodynamic Properties of Aqueous Sodium Chloride Solutions, J. Phys. Chem. Ref. Data. 13 (1984) 1–102. doi:10.1063/1.555709.
[52] M. Tedesco, A. Cipollina, A. Tamburini, I.D.L. Bogle, G. Micale, A simulation tool for analysis and design of reverse electrodialysis using concentrated brines, Chem. Eng. Res. Des. 93 (2015) 441–456. doi:10.1016/j.cherd.2014.05.009.
[53] M.L. La Cerva, M. Di Liberto, L. Gurreri, A. Tamburini, A. Cipollina, G. Micale, M. Ciofalo, Coupling CFD with a one-dimensional model to predict the performance of reverse electrodialysis stacks, J. Memb. Sci. 541 (2017) 595–610. doi:10.1016/j.memsci.2017.07.030.
[54] R. Ashu, S. Pawlowski, J. Veerman, K. Bouzek, E. Fontananova, S. Velizarov, J. Goulão, K. Nijmeijer, E. Curcio, Progress and prospects in reverse electrodialysis for

salinity gradient energy conversion and storage, 225 (2018) 290–331. doi:10.1016/j.apenergy.2018.04.111.
[55] I. Statistics, Capital Cost Estimates for Utility Scale Electricity Generating Plants, (2016).
[56] L. Henthorne, B. Boysen, State-of-the-art of reverse osmosis desalination pretreatment, Desalination. 356 (2015) 129–139. doi:10.1016/j.desal.2014.10.039.
[57] S. Loutatidou, B. Chalermthai, P.R. Marpu, H.A. Arafat, Capital cost estimation of RO plants: GCC countries versus southern Europe, Desalination. 347 (2014) 103–111. doi:10.1016/j.desal.2014.05.033.
[58] M. Busch, W.E. Mickols, Reducing energy consumption in seawater desalination, Desalination. 165 (2004) 299–312. doi:10.1016/j.desal.2004.06.035.
[59] B. Pilat, Practice of water desalination by electrodialysis, Desalination. 139 (2001) 385–392. doi:10.1016/S0011-9164(01)00338-1.
[60] H. Strathmann, Assessment of Electrodialysis Water Desalination Process Costs, Proc. Int. Conf. Desalin. Costing, Lemassol, Cyprus, December 6-8, 2004. (2004) 32–54.
[61] S. Quoilin, S. Declaye, B.F. Tchanche, V. Lemort, Thermo-economic optimization of waste heat recovery Organic Rankine Cycles, Appl. Therm. Eng. 31 (2011) 2885–2893. doi:10.1016/j.applthermaleng.2011.05.014.
[62] U. Caldera, D. Bogdanov, C. Breyer, Desalination Costs Using Renewable Energy Technologies, in: V.G. GUDE (Ed.), Renew. Energy Powered Desalin. Handb., 1st ed., 2018: pp. 287–329.
[63] M. Tedesco, P. Mazzola, A. Tamburini, G. Micale, I.D.L. Bogle, M. Papapetrou, A. Cipollina, Analysis and simulation of scale-up potentials in reverse electrodialysis, Desalin. Water Treat. 3994 (2014) 1–13. doi:10.1080/19443994.2014.947781.
[64] L. Gurreri, A. Tamburini, A. Cipollina, G. Micale, CFD analysis of the fluid flow behavior in a reverse electrodialysis stack, 48 (2012) 390–403. doi:10.1080/19443994.2012.705966.
[65] L. Gurreri, A. Tamburini, A. Cipollina, G. Micale, M. Ciofalo, CFD prediction of concentration polarization phenomena in spacer- fi lled channels for reverse electrodialysis, J. Memb. Sci. 468 (2014) 133–148. doi:10.1016/j.memsci.2014.05.058.
[66] L. Gurreri, A. Tamburini, A. Cipollina, G. Micale, M. Ciofalo, Flow and mass transfer in spacer-filled channels for reverse electrodialysis: a CFD parametrical study, J. Memb. Sci. 497 (2016) 300–317. doi:10.1016/j.memsci.2015.09.006.

APPENDIX

A.1. Polarization coefficients

The solution concentrations at membrane interphase ($C_{H,m}$ and $C_{L,m}$) are different from the concentrations of the solution in the bulk (i.e., $C_{H,b}$ and $C_{L,b}$) due to polarization phenomena. In order to evaluate the real concentration of the solutions at the membrane interface, polarization coefficients for dilute and concentrate are defined as follow:

$$\theta_H(k) = \frac{C_{H,m}(k)}{C_{H,b}(k)} = 1 - \frac{2J_{tot}(k)\delta_H}{C_H(k)D_H(k)Sh_H(k)} \quad \text{(A.1)}$$

$$\theta_L(k) = \frac{C_{L,b}(k)}{C_{L,m}(k)} = \left(1 + \frac{2J_{tot}(k)\delta_L}{C_L(k)D_L(k)Sh_L(k)}\right)^{-1} \quad \text{(A.2)}$$

where D_H and D_L are the diffusion coefficients of dilute and concentrate; J_{tot} is the global salt flux across the IEM membrane, δ_L and δ_H the channel thickness (155 μm), Sh_H and Sh_L are the Sherwood numbers of concentrate and dilute in the kth element. Sh is evaluated using dimensionless correlations obtained from CFD simulations as function of Reynolds and Schmidt numbers [65,66]. For profiled membranes (OCF) [53], Sh numbers are evaluated as:

$$Sh(k) = (-1.3265\cdot10^{-6}\,\mathrm{Re}(k)^4 - 2.4408\cdot10^{-4}\,\mathrm{Re}(k)^3 - 1.1131\cdot10^{-2}\,\mathrm{Re}(k)^2 + 3.8707\cdot10^{-1}\,\mathrm{Re}(k) + 9.2319)\left(\frac{}{S}\right.$$

(A.3)

where Sc_{ref} is the Schmidt number of the reference solution, i.e., NaCl solution at 25°C,1 atm and 0.017 M.

From equations A.1 and A.2, the actual concentrations of the dilute and concentrate at the membrane interface for each calculation element are evaluated. Such concentrations are used to calculated related polarization factors θ. These factors are used in equation 3 and in the equation of water and salt fluxes to evaluate the real stack performance, taking into account the effect of polarization phenomena.

A.2. Pressure drops

The pressure drops in each discretization element are calculated with the following equation:

$$\Delta p(k) = \frac{1}{2}\frac{\Delta x}{D_{eq}} f_{Darcy}(k)\rho_{av}(k)v_{av}(k)^2 \quad \text{(A.4)}$$

where D_{eq} is the equivalent diameter (i.e. 2 times the channel thickness δ), ρ_{av} and u_{av} are the average velocity and density of the solution within the calculation element, Δx is the length of the discretization element, f_{Darcy} is the friction factor. The friction factor values are obtained from CFD simulations as function of the *Re* number and channel properties, as reported in [65]. Suitable correlations of f_{Darcy} as a function of the Re number in the channels of profiled membranes (OCF) can be obtained by fitting CFD results [53].

$$f_{Darcy}(k) = (6.0719 \cdot 10^{-3}\,\mathrm{Re}(k) + 2.3907) \cdot \frac{96}{\mathrm{Re}(k)} \qquad \text{(A.5)}$$

The overall pressure drop within the stack is obtained as the sum of the pressure drop of the single discretization element for dilute and concentrate streams. In formula:

$$P_{loss} = P_{loss,H} + P_{loss,L} = \sum_{k}^{N_k} \Delta p(k)_H + \sum_{k}^{N_k} \Delta p(k)_L \qquad \text{(A.6)}$$

A.3. Membrane properties

The average permselectivity and membrane resistance of Fujifilm® type 10 membranes as a function of solution concentration in the case of NaCl solutions (results provided by Fujifilm®) are reported as a function of solution concentration in equation A.7 and A.8:

$$\alpha_{av}(x) = 0.987 - 0.0441\, C_H(x) - 0.183 C_L(x) \qquad \text{(A.7)}$$

$$R_{IEM,av}(x) = 0.487\, C_H^2(x) - 2.81\, C_H(x) + 7.21 - 0.14\, C_L(x) \qquad \text{(A.8)}$$